INFORMATION TO USERS

This dissertation was produced from a microfilm copy of the original document. While the most advanced technological means to photograph and reproduce this document have been used, the quality is heavily dependent upon the quality of the original submitted.

The following explanation of techniques is provided to help you understand markings or patterns which may appear on this reproduction.

1. The sign or "target" for pages apparently lacking from the document photographed is "Missing Page(s)". If it was possible to obtain the missing page(s) or section, they are spliced into the film along with adjacent pages. This may have necessitated cutting thru an image and duplicating adjacent pages to insure you complete continuity.

2. When an image on the film is obliterated with a large round black mark, it is an indication that the photographer suspected that the copy may have moved during exposure and thus cause a blurred image. You will find a good image of the page in the adjacent frame.

3. When a map, drawing or chart, etc., was part of the material being photographed the photographer followed a definite method in "sectioning" the material. It is customary to begin photoing at the upper left hand corner of a large sheet and to continue photoing from left to right in equal sections with a small overlap. If necessary, sectioning is continued again — beginning below the first row and continuing on until complete.

4. The majority of users indicate that the textual content is of greatest value, however, a somewhat higher quality reproduction could be made from "photographs" if essential to the understanding of the dissertation. Silver prints of "photographs" may be ordered at additional charge by writing the Order Department, giving the catalog number, title, author and specific pages you wish reproduced.

University Microfilms

300 North Zeeb Road
Ann Arbor, Michigan 48106

A Xerox Education Company

INTERFACIAL AND MORPHOLOGICAL PHENOMENA

IN

POLYSTYRENE LATEX SYSTEMS

by

PRESTON KEUSCH

A dissertation submitted to the Graduate Faculty in Engineering in partial fulfillment of the requirements for the degree of Doctor of Philosophy, The City University of New York.

1973

This manuscript has been read and accepted by the Graduate Faculty in Engineering in satisfaction of the dissertation requirement for the degree of Doctor of Philosophy

1/29/73
Date

David J. Williams
Chairman of Examining Committee

1/29/73
Date

Jacques E. Benveniste
Executive Officer

Professor Robert A. Graff

Professor Irving Waltcher

Professor David J. Williams
Chairman

Professor Joseph Yerushalmi

Supervisory Committee

The City University of New York

ABSTRACT

The long standing assumption of component and reaction homogeneity within the growing latex particle in styrene emulsion polymerization was recently challenged by Grancio and Williams (J. Polymer Sci., A-1,8,2617 (1970)). They postulated that the growing particle possessed a core-shell structure, comprised of a polymer-rich core surrounded by a monomer-rich shell which served as the major locus of polymerization. The research described herein verifies the core-shell model, extends its applicability over a range of conditions relevant to emulsion polymerization and presents a theoretical basis for its occurrence.

Confirming evidence for the core-shell structure was accomplished by conducting seeded styrene polymerizations in which the second stage of growth was initiated only after the monomer charge had attained equilibrium saturation with seed polymer. The second generation polymer was distinguished from the first using two tagging-identification procedures: (i) trace-butadiene tagging coupled with ultramicrotomy and osmium tetroxide staining and (ii) tritiated-styrene tagging coupled with electron microscope autoradiographic detection. Substantive evidence confirming the core-shell postulate was obtained by both procedures. Prevalence of the core-shell morphology was found over an extended range of conditions

relevant to emulsion polymerization: (i) molecular weight (from 0.02×10^6 to 10.0×10^6, viscosity average), (ii) particle diameter (from ca. 500 Å to 6500 Å), (iii) initiator type (water soluble and oil soluble), and (iv) butadiene level in the second stage of growth (from 0.7 wt-% to 50 wt-%).

From a theoretical point of view we have for the first time correctly assessed the importance of the particle-water interface in controlling the solution thermodynamics, kinetics, and morphology within the interior of these colloidal particles. Using current statistical mechanical models of high polymers attached to inpenetrable, noninteracting interfaces, we show that the polymer segments will tend to be repelled by the interface leaving a surface excess of solvent. Since the foregoing conditions are met in the styrene-polystyrene latex system, we believe that constraints on the macromolecular conformations within the particle to be the underlying factor determining the core-shell structure.

The technological implications of the core-shell phenomenon have also been studied. Overcoating latexes by staged monomer addition is widely used industrially to tailor the properties of latexes. Our findings suggest that overcoating is controlled by the same mechanisms that we have found to govern the core-shell mode of growth.

ACKNOWLEDGMENTS

I thank Professor David J. Williams for his exceptional guidance, interest and inspiration concerning this research and in my overall education. I thank Mr. John Bodnaruk for his assistance in instructing me on the techniques of electron microscopy and Mr. Joseph Prince for his assistance in developing the copolymer emulsion polymerizations. I thank as well J. Cohn, T. Naaber, D. Greer and D. J. Keusch for their help in manuscript preparation and photo production for the documents that emanated from this study. This work was supported by the National Science Foundation under grant NSF GK 17582.

TABLE OF CONTENTS

TABLE OF CONTENTS (cont.)

TABLE OF CONTENTS (cont.)

LIST OF FIGURES

LIST OF FIGURES (cont.)

LIST OF FIGURES (cont.)

LIST OF FIGURES (cont.)

LIST OF FIGURES (cont.)

LIST OF FIGURES (cont.)

LIST OF TABLES

LIST OF TABLES (cont.)

I. INTRODUCTION

Since the first definitive papers (1,2,3) attempting to elucidate the mechanisms operating in styrene emulsion polymerization, the growing monomer-polymer particle has generally been envisioned as a homogeneous entity, with monomer and polymer uniformly distributed and with no specific locus of polymerization. This long standing viewpoint was challenged recently by Grancio and Williams (4,5). They postulated that the growing particle possessed a core-shell structure, comprised of a polymer-rich core surrounded by a monomer-rich shell which served as the major locus of polymerization. Their model was derived from kinetic studies utilizing continuously uniform styrene emulsion polymerizations that followed Smith-Ewart, case 2 kinetics. Confirming evidence was obtained by electron microscope observation of ultra-thin sections of latex particles.

This unorthodox view demanded independent verification and further investigation to determine the range of conditions over which this phenomenon might prevail. The experiments, forming the foundation of this dissertation and designed to meet the foregoing demands, were based on a series of seeded styrene emulsion polymerizations in which the second stage of growth was initiated only after the second stage monomer charge had attained equilibrium saturation with the seed latex.

Another important condition was that the second stage monomer (monomer II) and the polymer generated therefrom (polymer II) were compatible with the seed polymer (polymer I). The latex morphology at completion was determined by electron microscope observation, using two independent means of distinguishing between polymers I and II: (i) trace-butadiene tagging coupled with ultramicrotomy and osmium tetroxide staining, and (ii) tritiated-styrene tagging coupled with autoradiographic detection (6). We have found by both procedures substantive evidence confirming the core-shell postulate. The core-shell morphology was found to prevail over a wide range of conditions relevant to emulsion polymerizations: (i) molecular weight (from 0.02×10^6 to 10.0×10^6, viscosity average), (ii) particle diameter (from ca. 500 Å to 6500 Å), (iii) initiator type (water soluble and oil soluble), and (iv) butadiene level in polymer II (from 0.7 wt-% to 50 wt-% based on monomer II).

For the styrene-polystyrene system under study, a heterogeneous monomer-polymer particle seems indeed remarkable inasmuch as the components are mutually soluble in all proportions in systems of macroscopic size. In retrospect, past investigators seemed justified in presuming that for such a latex system monomer and polymer were uniformly mixed within the particle. In making this assumption, however, an important facet of the

system had been overlooked. That is, latex particles are polymer colloids with large interfacial area to volume ratios.

We have for the first time correctly assessed the importance of the particle-water interface in controlling the solution thermodynamics, kinetics, and the morphology of the particle interior. The fact that the core-shell morphology was found to emanate from conditions of saturation equilibrium prompted us to analyze the system from a molecular thermodynamic point of view. Analysis was based on recent developments in describing the statistical behavior of polymer segments near surfaces (7,8,9). An integral component of the analysis was the fact that nearly all polymer chain ends in emulsion polymerization are bound to the particle surface (10,11) In general, a long chain molecule attached to an inpenetrable, noninteracting interface will tend to have its segments repelled from the interface, thereby leaving a surface excess of solvent. Analysis of the energetics for the foregoing system shows that conditions of polymer segment deficiency near the interface are thermodynamically favored compared to polymer segment crowding. The analogy for latex systems is direct, i.e., polymer segments will be retracted from the inpenetrable, noninteracting particle surface to give minimum system free energy. Finally, the actual monomer saturated latex system is shown to have a polymer segment density

distribution that is high in the center and low in the peripheral region. Thus, we have placed the inhomogeneously swollen latex model on a firm theoretical foundation.

The core-shell phenomenon has technological implications that also merit consideration. Overcoating latexes by staged monomer addition is widely used to tailor the properties of latexes. In this process, polymer II is of a different composition than polymer I. Polymer I is usually compatible with monomer II but not with polymer II. In practice, monomer II is added to seed polymer I by programmed addition. Until now it has been thought that overcoating is controlled by the slow monomer addition and that the polymer-polymer incompatibility enhances this process. Our findings suggest that overcoating is controlled by the same mechanisms that we have found to govern the core-shell mode of growth.

II. ORIGINS OF THE CORE-SHELL CONCEPT

The first insights into the mechanisms operating in emulsion polymerization appeared in the 1940's with the pioneering work of Harkins (3) and of Smith and Ewart (2). Their contributions are developed here to the extent necessary to reveal how the work of Grancio and Williams advances our understanding of styrene emulsion polymerization. In brief preview, the work of Grancio and Williams (4) put the Smith-Ewart case 2 theory on a more rational basis and gave new insights into the mechanisms operating in styrene emulsion polymerization. Additionally, their work provides the basis and motivation for this study.

A. Constant-Rate Styrene Emulsion Polymerization

The core-shell model was first proposed on the basis of kinetic studies of constant-rate styrene emulsion polymerization. In order to properly develop the background for our current work, we dwell extensively on this mode of polymerization.

In typical styrene emulsion polymerizations, the conversion time-curve, as schematically presented in Figure 1, describes three stages of growth: Stage I is characterized by concurrent latex particle nucleation and growth so that an increasing rate is observed. Concurrent nucleation and growth also lead to particle size distribution in the latex product. In stage II a constant polymerization rate is observed as the particles nucleated in stage I continue to grow. For reasons that will be described shortly, the particles reach their approximate final size during this stage at about 25 to 30% conversion. Stage III begins at 55 to 60% as the conversion-time curve deviates from linearity; the rate may increase or decrease depending on whether or not the Trommsdorff effect is important. With this abbreviated overall view we now dwell extensively on constant-rate behavior, the specific objective of this study.

Figure 1

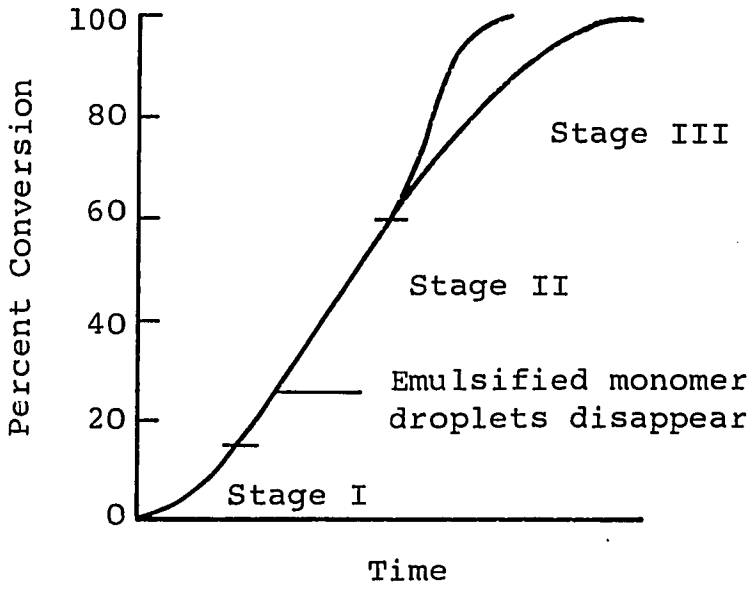

Typical percent conversion vs. time curve for styrene and styrene-like emulsion polymerizations of the GR-S type.

The foregoing description and much of what is to follow is generally applicable to formulations of the GR-S* type (2) which are comprised of 180 parts (by weight) water, 100 parts water-soluble monomer (such as styrene), 3 to 5 parts fatty acid soap, and 0.3 to 0.5 parts water soluble initiator (such as potassium persulfate).

Figure 2 depicts the state of affairs during the early part of stage II when three phases are present: growing latex particles, emulsified monomer droplets, and the aqueous phase which serves as the suspending medium. The hydrophobic phases are stabilized by an adsorbed layer of surfactant. The latex particles serve as the major loci of polymerization. As monomer is converted to polymer within these particles, additional monomer is supplied to them via aqueous diffusion from the emulsified monomer droplets. At 25 to 30% conversion the supply of monomer from these reservoirs is exhausted; consequently, the latex particles attain their approximate final size at this point in the reaction. The latex particles usually range from a few hundred angstroms in diameter at nucleation to a thousand or several thousand angstroms at completion.

* Government rubber-styrene: a copolymer comprised of 75% butadiene and 25% styrene.

Figure 2

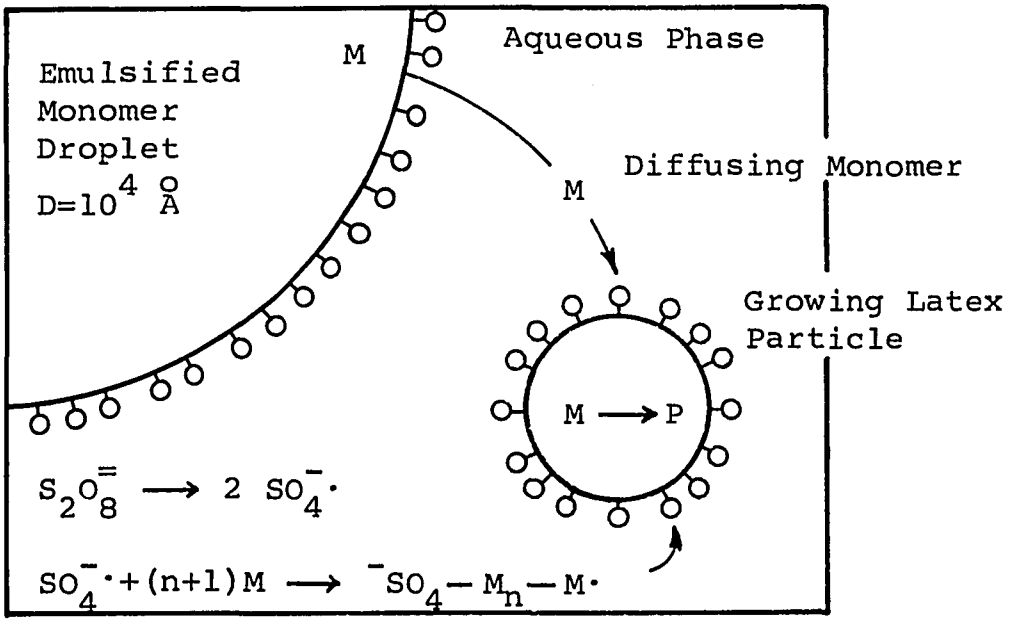

Illustration of the stage II growth period in styrene emulsion polymerization.

In addition to serving as a suspending medium and the transport medium for monomer diffusion, the aqueous phase serves as the source of freee radicals. The water soluble initiator potassium persulfate is generally used. This initiator decomposes thermally by the first order mechanism to form water-soluble, sulfate-radical anions.

$$S_2O_8^{=} \xrightarrow[50\text{-}65^{o}\ C]{heat} 2SO_4^{-}\cdot$$

These free radicals then react with the limited monomer dissolved in the aqueous phase to form soap-type, anionic free radicals,

$$SO_4^{-}\cdot + (n+1)CH_2{=}CX_2 \longrightarrow {}^{-}SO_4\text{-}(CH_2\text{-}CX_2)_n\text{-}CH_2\text{-}CX_2\cdot$$

After a short time, while n is still small, these soap-type free radicals become sufficiently hydrophobic to enter the interface of the oil phase, thereby initiating (or terminating) growth within the particles.

In a typical emulsion polymerization, there are about 10^{14} latex particles/cc . The initiator concentration is such that the rate of free radical generation is about 10^{12} to 10^{13} free radicals/cc-sec . Thus, free radicals enter the growing particles on the average, once every 10 to 100 seconds. The growth profile of a latex particle is shown in the bar-diagram of Figure 3 where the rate of polymerization per particle is plotted against time for the three rates of particle initiation, R_{ip}, $2R_{ip}$, and $3R_{ip}$. In each case when

Figure 3

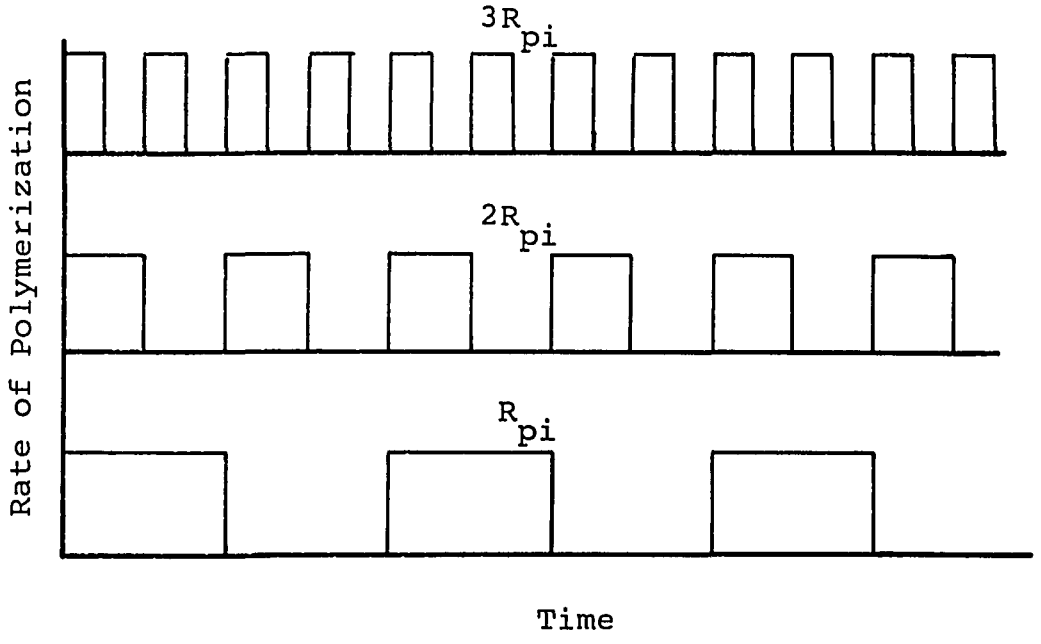

Bar diagram showing the effect of rate of particle initiation, R_{pi}, on the rate of particle conversion, R_{pp}

a radical enters R_{pp} jumps from zero to a constant value; growth proceeds until another free radical enters via the usual mechanism, and virtual instantaneous termination occurs between the existing and entering radicals. Thus constant-rate growth within an individual latex particle is characterized by alternating periods of activity and inactivity. (In a real situation, the periodicity would not be as regular as depicted, but one would find a distribution, which leads, in turn to a molecular weight distribution. The regular periodicity displayed here, however, does not influence the argument.)

Deviations from the foregoing are encountered with vinyl acetate which is relatively water soluble and has a high transfer coefficient (13), and with vinyl chloride a system in which the polymer is insoluble in the monomer and which has a high transfer coefficient. Both transfer mechanisms allows radicals to desorb from latex particles —— which can later re-absorb.

The measureable overall rate of polymerization, R_p, is given by

$$R_p = N_p R_{pp} \tag{1}$$

where N_p = the number of growing latex particles and R_{pp} = the rate of polymerization per particle. If R_{pp} is constant, then we should recognize that R_p increases during stage I because N_p is increasing. Thus, if we focus our attention on the intrinsic polymerization reactors —— i.e., the growing latex particles —— we see that constant-rate behavior is actually

observed from zero percent conversion rather than just from 15%.

Constant-rate growth is best displayed in uniform particle size systems in which the conversion-time curve is linear over an extended conversion range (14,15). In uniform systems nucleation is controlled such that the particles are all nucleated over a very short interval, rather than over a a period of time. The particles are virtually all uniform in size to begin with, and competitive growth (16) further enhances the uniformity*. As a consequence of virtual instantaneous nucleation, uniform systems do not exhibit a stage I period. Uniform systems also provide another advantage in kinetic studies of emulsion polymerization; namely, increased analytic accessibility over their polydispersed counterparts. In general, we must expect that such kinetic parameters as R_{pp}, R_{ip} and particle monomer concentration will depend on particle size. With uniform systems these parameters can be precisely evaluated by experiment.

The kinetic studies which led Grancio and Williams to postulate the core-shell particle structure were based on these uniform-type systems. The two formulations employed are tabulated below. The only difference between these and the GR-S formulations previously cited is in the types and

* Figures 1 to 4 in reference 14 show this developing uniformity in a series of electronmicrographs of latex particles at various stages of growth.

amounts of soaps used. Other than the elimination of stage I, the mechanism of polymerization of uniform latices follows that outlined here. The underlying theory behind generating uniform latices is clearly outlined by Bobalek et al. (17,18). The principle of using uniform latices in kinetic studies was first stated by Williams et al. (14,15). The most recent study of the practical side of this art is reported by Woods et al. (19).

Table I

Formulations For

Constant-rate (0-60%C) Uniform Particle

Size Styrene Emulsion Polymerizations

100 grams	Styrene Monomer		
180	Distilled Water		
0.5	$K_2S_2O_8$		
3.0	Triton X-100		
0.075	KOH (pH=9.0)		
Sodium Lauryl Sulfate		0.3 gram	0.15 gram
	R_p	13%/hr	21%/hr
	D_p	1950 Å	2300 Å
	N_p	5.2×10^{13}/ml	8.8×10^{13}/ml

The formulations shown in Table I exhibit Smith-Ewart, case 2 kinetics (1) from zero to about 60% conversions. The

amounts of anionic soap resulted in the two tabulated sets of values for N_p and consequently R_p and D_p, the final particle diameter. The rate curves are shown in Figure 4. These curves are plotted against a shifted time scale so that each curve can be displayed separately in a concise fashion.

Figure 4

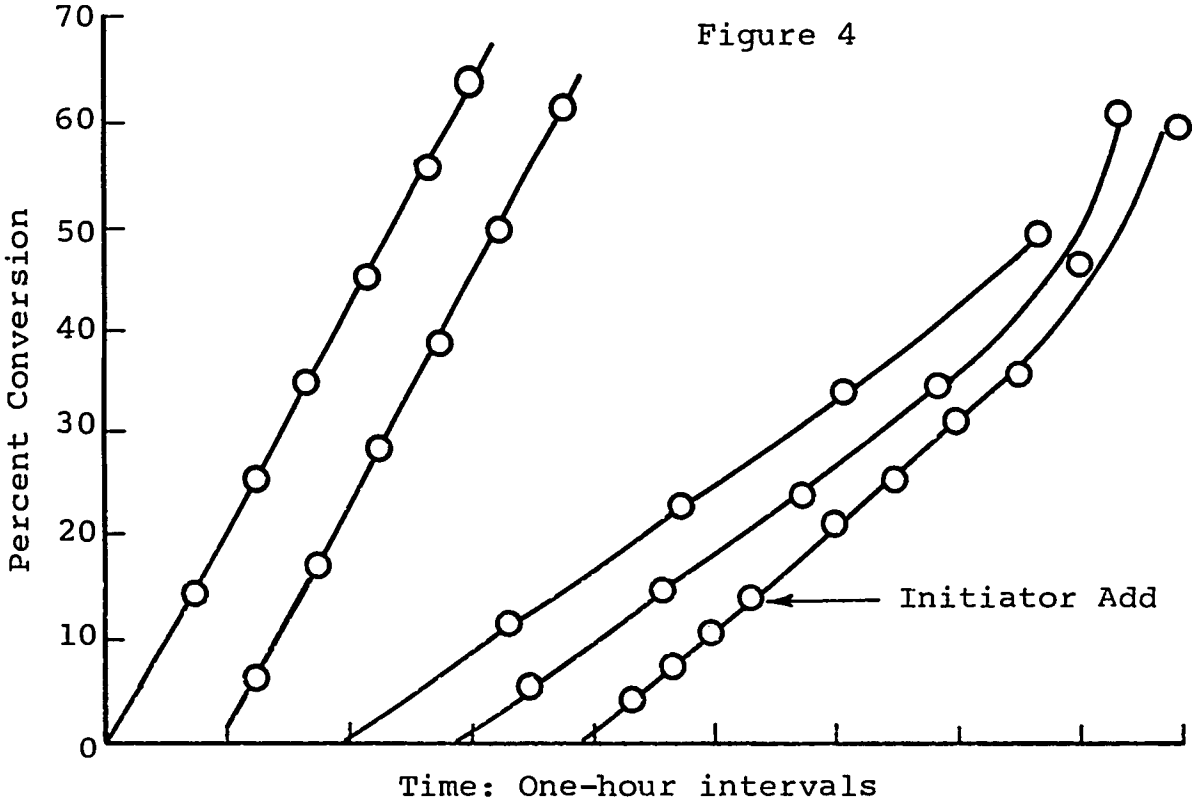

Percent conversion vs. time curves for 13%/hour and 21%/hour runs (4).

B. Smith-Ewart, Case 2 Kinetics

Constant-rate growth can be described in terms of the Smith-Ewart theory, case 2 (1), in which the rate of polymerization per particle, R_{pp}, is expressed as

$$R_{pp} = k_p \bar{n}[M] \quad (2)$$

where k_p is the propagation constant, [M] is the monomer concentration within the particle, and $\bar{n}$ is the average number of free radicals per particle. With the growth profile described by the bar diagram in Figure 3, we see that the particles contain free radicals half the time, or $\bar{n}$ the average number of free radicals per particle = 1/2. With $\bar{n}$ = 1/2 and constant, the rate of polymerization per particle is constant and independent of particle size, provided [M] is constant. It should be noted that Equation 2 is identical in form to the more familiar expression for the rate of propagation, i.e., $-d[M]/dt = k_p[A][M]$ where [A] = the active species concentration.

Evidence for $\bar{n}$=1/2 and constant has been provided by initiator perturbation studies which are rather direct and convincing (4,20). As shown in Figure 4, for curve E, the initiator concentration of a run in progress was suddenly increased during its constant rate period. In concordance with the rationale associated with Figure 3, the observed invariance in the rate is evidence of $\bar{n}$=1/2 and constant.

That is, an increase in initiator concentration should change only the frequency of growth of a latex particle as shown in Figure 3 and not its rate.

For the most part, the behavior of [M] has been examined in equilibrium swelling experiments in which fresh monomer is added to a latex until the particles reach their equilibrium capacity. These studies (21,22,23) show the equilibrium capacity of the particles, $[M]_{eq}$, to be a weakly increasing function of particle size, with $[M]_{eq}$ ordinarily ranging from 0.67 to 0.80 for styrene. Furthermore, the disappearance of emulsified monomer has been observed (visually) at about 30% conversion (22). With these two observations coupled with the requirements of Equation 2 as a basis, it has been commonly maintained that the latex particles are swollen to capacity and that $[M]_{eq}$ is constant during constant-rate growth. As a consequence, the Smith-Ewart theory was mistakenly thought to be applicable only at small particle sizes and low conversions during stage I and stage II up to about 30%. This pattern of thought has resulted in a considerable effort to describe mathematically how $\bar{n}$ might increase with increasing particle size and viscosity as the reaction progresses beyond the point where the Smith-Ewart theory is deemed no longer valid (24-27). The "apparent" constant-rate behavior beyond about 30% has been tentatively

explained as resulting from a fortuitous balance between increasing $\bar{n}$ and decreasing [M] (24-29).

The earliest studies by Harkins et al. (3,30) on the behavior of [M] were based on direct measurement of [M] during the progress of a run rather than on measurement of $[M]_{eq}$. These studies actually showed [M] to be a continuously decreasing function of conversion even during periods of constant rate.

The findings of Harkins et al., and the apparent ability of the emulsion polymerization reaction to sustain a constant rate beyond 30%, despite a declining value of [M] and its implications with regard to Equation 2, prompted Grancio and Williams to perform dynamic measurements.

Shown in Figure 5 are the results of their dynamic measurements of the particle monomer concentration, plotted as weight fraction monomer $[M]_w$ versus percent conversion. For the 13%/hr formulation $[M]_w$ = 0.73 and constant up to 27% when the emulsified monomer disappeared. In the 21%/hr formulation, $[M]_w$ decreased continuously from an initial value of 0.8-0.7 when the emulsified monomer disappeared. In both cases, of course, $[M]_w$ decreased continuously beyond 30% conversion. The variations of $[M]_w$ in these runs stands in striking contrast to the extended constant rate period (0 to 60%) exhibited by these formulations and to the requirements of Equation 2.

A rather straightforward scheme was proposed (4) to resolve the foregoing dilemma. From Equations 1 and 2 since

Figure 5

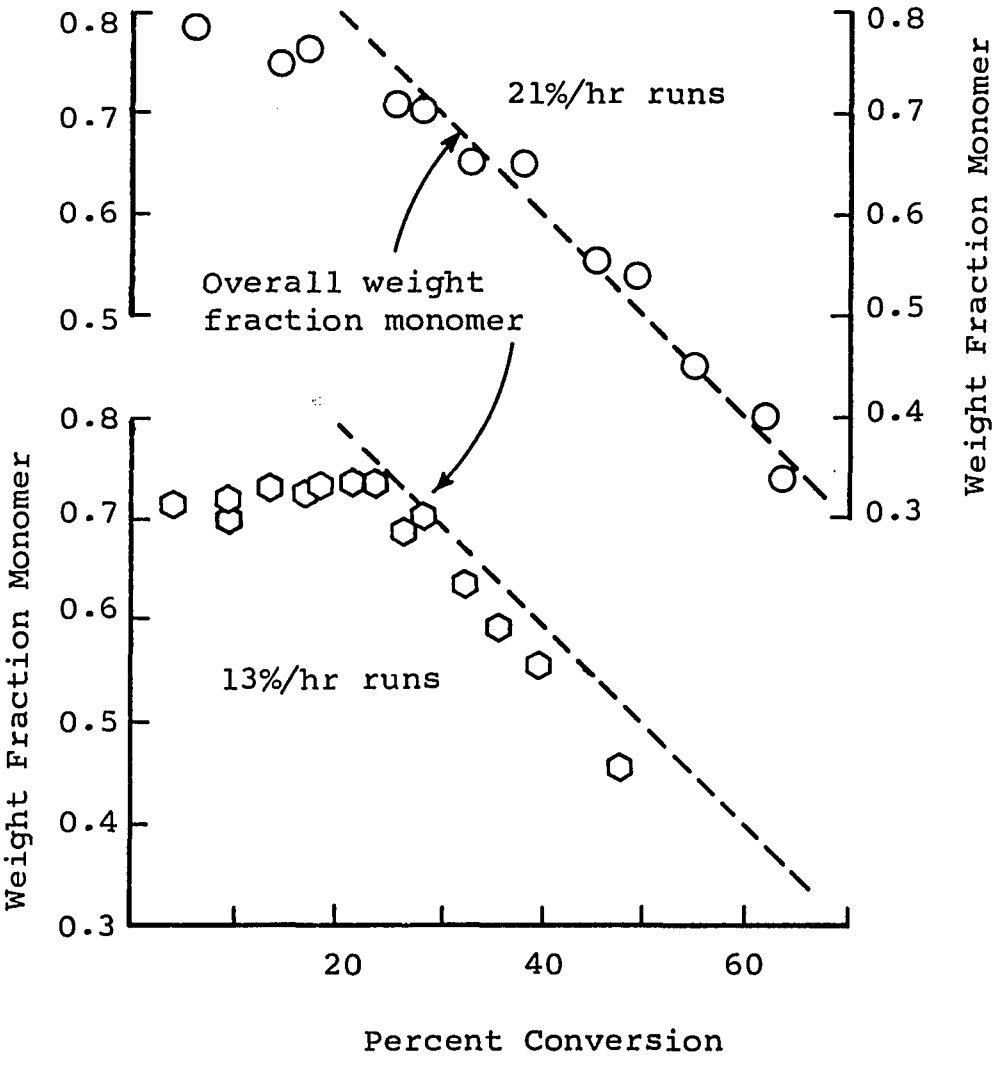

Weight fraction monomer in latex particles vs. percent conversion for 13%/hr and 21%/hr runs (4).

N_p, R_{pp}, $\bar{n}$ and k_p are constant, [M] must be constant at the actual site of polymerization. A particle in which monomer is uniformly distributed cannot simultaneously satisfy the requirements of Equations 1 and 2 and the observed behavior of [M]. From this, it follows that the growing particle is heterogeneous, that a zone of essentially constant monomer concentration exists within the particle during constant rate polymerization, and that the zone serves as the major locus of polymerization. Such a requirement is satisfied by a concentric sphere morphology, consisting of a polymer-rich core surrounded by a monomer-rich shell; the major locus of polymerization is the outer shell where a Smith-Ewart mechanism prevails. With such a core-shell morphology the changing overall particle monomer concentration is consistent with constant particle conversion rates because reaction takes place in an essentially pure monomer environment in the peripheral region of the particle.

In addition, Grancio and Williams performed the following experiment that provided physical evidence for the core-shell morphology (4). To a 13%/hr styrene run at 20% conversion, a portion of butadiene was charged. They expected that copolymerization would result, and if the model were correct, that the final latex particle should consist of a pure polystyrene core —— corresponding to the polymer core which existed when the butadiene was charged —— surrounded by a spherical styrene-butadiene copolymer shell. Since the unsaturated butadiene repeat

unit could be stained with osmium tetroxide, an ultrathin cross-section taken through the center of the particle should appear as a doughnut shape under electron microscope observation. Figure 6 shows a thin section taken from such a particle; it clearly shows the expected unstained core and the stained ring.

Figure 6

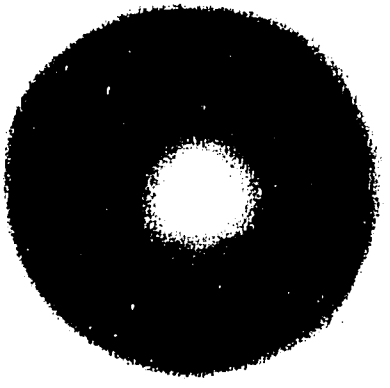

Ultra-thin section of latex particle showing core-shell morphology (250,000X) Reference (4).

C. Motivation for this Work

The core-shell model, with its extensive technological and fundamental implications, called for further investigation. Since Grancio and Williams studied a single system under only two sets of conditions, with limited data, it was necessary to verify their conclusions by independent experiments and to establish the range of conditions over which the model is valid. Furthermore, the core-shell model as stated in its original form is entirely phenomenological. Thus, a goal of this study was to ascertain factors governing the core-shell model and to present a mechanistic model in accordance with accepted macromolecular theory.

III. VERIFICATION AND EXTENSION OF THE CORE-SHELL MODEL

A first consideration in our experimental program was to determine whether the core-shell morphology was controlled by equilibrium factors or by kinetic factors. Prevalence of the core-shell mode of growth in situations where monomer II is in a state of equilibrium saturation with polymer I, would argue in favor of control by thermodynamic factors. Knowing that the core-shell morphology emanates from a state of thermodynamic equilibrium additionally directed us to investigate the molecular thermodynamic theory that would pertain to swollen latex particles. We discuss the latter approach in a later chapter.

In preview, this chapter describes the definitive part of our experimental work in which we have performed the equilibrium seeding experiments: (i) trace-butadiene tagging, and (ii) autoradiography. Both experiments verify the core-shell morphology and show that it emanates from conditions of equilibrium. We then present the range of conditions over which the core-shell morphology prevails. The parameters studied were seed molecular weights, particle size, and polymer-polymer incompatibility level. We conclude the chapter by discussing the technological implications of the core-shell model.

A. Seeded Polymerizations 1: Butadiene Tagging

Up to this point arguments suggesting and supporting the core-shell model have been based on evidence obtained in kinetic studies (4). One might wonder, however, whether particle morphology is governed by molecular-thermodynamic factors or by diffusional factors arising during latex growth. With reference to the latter, one could argue, for example, that the core-shell morphology might prevail if the rate of polymerization is very much faster than the rate of diffusion of monomer to the site of polymerization. In this work we present experimental evidence and theoretical arguments which support the case for control of particle morphology by molecular-thermodynamic factors.

In order to elucidate the factors controlling latex particle morphology we undertook seeded polymerizations of the following kind: To a previously prepared latex seed (polymer I) still in aqueous suspension, charge fresh monomer (monomer II) with a trace of butadiene until the particles attain equilibrium saturation. Reinitiate polymerization, and convert monomer II to polymer II. Destabilize the final latex product; isolate and embed the particles in epon resin; and obtain thin cross-sections by ultramicrotomy. Expose the thin sections to osmium tetroxide and examine them in the electron microscope. During the saturation phase of this

experiment the butadiene should distribute within the latex particle in direct proportion to monomer II, and it should copolymerize with styrene in its normal random fashion. Since the residual unsaturation in the butadiene repeat unit can be stained by osmium tetroxide, the butadiene serves to tag the second generation polymer, thereby establishing the location of polymer II within the thin cross-sections. The most important aspect of the foregoing experimental scheme is that polymerization is resumed only after monomer II and polymer I have attained a distribution within the latex particle which is characteristic of the equilibrium saturation state. In such an experiment we are suppressing any diffusional factors which might arise in a normal single stage polymerization. Also we ought to be able to make some inferences as to the equilibrium distribution of monomer II and polymer I from the final distribution of polymer I and polymer II —— a major objective of this work.

Experimental

In order to suppress any artifacts that might develop because of incompatibility between first generation poly-styrene and the second generation poly(styrene-co-butadiene), the butadiene level was maintained at less than 0.7 wt-% based on the final total polymer content. Thin films of the

final latex polymer were prepared by casting a 1% amyl acetate solution over water. Grids were placed on the floating film and them picked up in such a way as to carry off the cast film. These specimens were dried, exposed to osmium tetroxide, and examined by electron microscopy. Evidence of incompatibility was never observed.

In this phase of the study, the polymerizations were conducted in 300 ml bottles in a bottle polymerizer thermostatted for 65°C. We used the formulations described by Woods et al. (19,31) which produce monodispersed latexes. Sample formulations for both an unseeded and seeded polymerization are given in Appendix I. All batches were formulated at room temperature. The only variation we employed from the procedures described by Woods et al. were to be certain that we operated at or just below the saturation content of monomer in the two-stage polymerizations and to allow sufficient time (48 hours) to reach equilibrium before the resumption of polymerization.

The equilibrium saturation content of monomer for a latex was established by placing various amounts of monomer in a series of vials all containing the same amount of latex —— ca. 10% solids content; the vials were rocked gently for 48 hours at room temperature and then centifuged for several minutes; the highest monomer content at which

no supernatant monomer layer appeared after centrifugation established the equilibrium saturation content. No variation in the established value was observed when higher (ca. 15%) or lower (ca. 5%) solids contents were used. The equilibrium saturation content for the latex seeds employed here was about 73 wt-%. As it turns out, the saturation monomer content we determined was the same as that prescribed for the second stage charge by Woods et al.

To be certain that no artifacts would arise because of any polymerization that might occur during saturation, we checked for this possibility. Several blank samples of accurately known solids content were saturated with monomer for 48 hours; the inhibitor, paraquinone, was then added; and the samples were evaporated to dryness. No change in solids content was observed. Also, the intrinsic viscosity of the polymer was found to be the same before and after saturation. Hence, seed polymer remains unchanged during the saturation process, and it is unlikely that any artifacts could be introduced during this phase of batch preparation.

The ultra-thin cross-sections were obtained as follows. The repolymerized latices were destabilized from the emulsion, filtered, washed with methanol, then distilled water and finally dried. The dried latices were then mixed with the

embedding resin "Epon 812", (distributed by Ladd Research, Burlington, Vermont), placed in a mold suitably shaped for microtomy and allowed to cure according to standard techniques (32, 33). Upon curing, the mold was secured in the sample holding stage of an LKB "Ultratome III", ultramicrotome (manufactured by LKB Productor, Stockholm, Sweden), and sliced in thicknesses of less than 200Å using a glass or diamond knife (32, 34). The thickness of the slice was determined visually by the diffraction pattern emitted from the slice. The slices were then collected on a distilled water surface and picked up on an electron microscope grid. In general, many slices had to be made by this random slicing procedure to insure that slices were obtained near the center of the encapsulated latex particles. Only those slices that were cut near their centers and artifact free, i.e. essentially without knife chatter or distortion, were analyzed.

Results

The core-shell morphology is clearly evident in Figures 7 through 9. These figures show typical cross-sections prepared by the sectioning methods previously described. (Table II lists the run number and location of stain). In run 1-12-1 (Figure 7) the seed contained the

trace of butadiene and polymer II is pure polystyrene. In 1-33-1 (Figure 8) only polymer II contained the butadiene tracer. Figure 9, the result from run 1-27-1, is rather unusual. It shows a cross-section of a particle grown in three stages. Stages II and III were initiated under conditions of saturation equilibrium and trace quantities of butadiene were charged in stages I and III.

Note too that in all saturation runs the dimensions of the core observed by electron microscopy coincided, within experimental error (ca. 50Å), with the dimensions of the seed particles used in each run. It is difficult, of course, to always obtain center-cut cross-sections. In many instances we utilized cuts that were off-center. For the latter instances the true core-shell dimensions were obtained from simple geometric considerations of sliced concentric spheres using the formula:

$$D_1 = \sqrt{D_1'^2 + D_o^2 - D_o'^2} \qquad (3)$$

where D_1' = sliced shell diameter at cut off-center

D_o = true core diameter

D_o' = sliced core diameter at cut off-center

The results of these calculations are presented in Table III for the sliced encapsulated latex particles of Figures 7 through 9. It is seen that the calculated outer diameter D_1

Figure 7

Ultra-thin section of latex particle prepared by two-stage seed polymerization, with trace-butadiene in the seed. (Core stained, shell unstained) core/shell diameters : 1930A°/3070A°

Figure 8

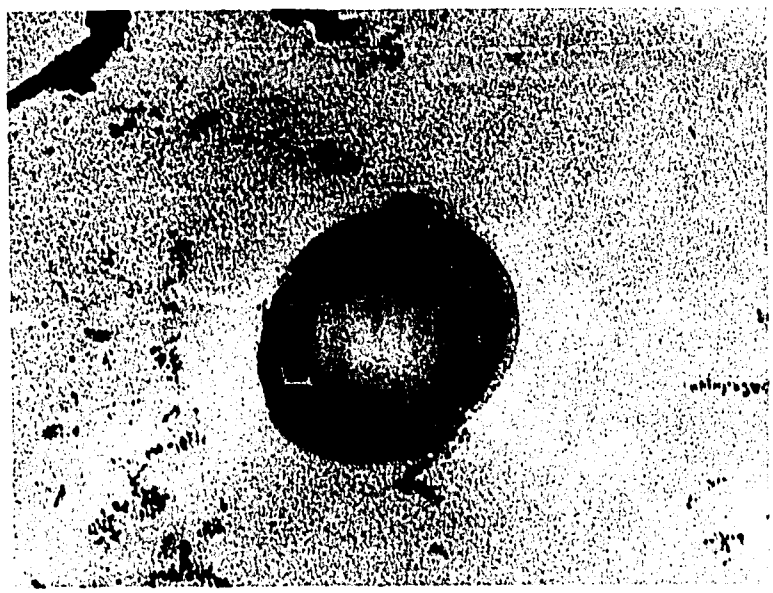

Ultra-thin section of latex particle prepared by two stage seed polymerization, with trace-butadiene added to monomer II. (Shell stained, core unstained) core/shell diameters : 5330A°/6430A°

Figure 9

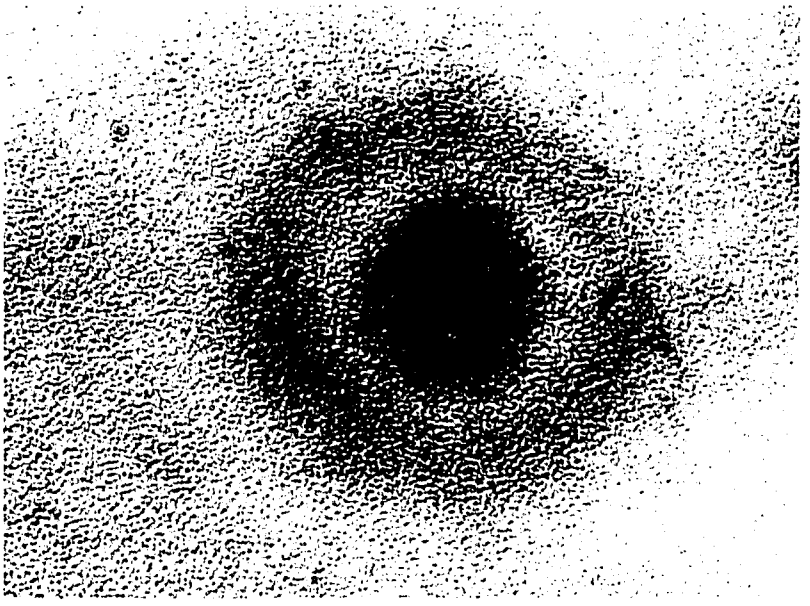

Ultra-thin section of latex particle prepared by three stage seed polymerization with trace-butadiene in the seed and added to monomer III. core/shell 1/shell 2 off-center slice diameters: 720 Å/1280 Å/2190 Å

Table II

Runs Verifying The Core-Shell Morphology

Run	Sizes			Location of Stain	Figure Number
	Core Å	Shell I Å	Shell II Å		
1-12-1	1930	3070	none	Core	7
1-33-1	5330	6430	none	Shell	8
1-27-1	1930	3070	4190	Core and Outer Shell	9

Table III

Comparison of Shell Dimensions in Whole and Sliced Particles

Run	D_o Core Diameter (Å)	D'_1 Sliced Outer Diameter (Å)	D'_o Sliced Inner Diameter (Å)	D_1 Calculated Shell Diameter (Å)	D_1 expt measured Shell Diameter (Å)
1-12-1	1930	3000	2000	2950	3020
1-33-1	3525	5410*	3800*	6560	6500
1-27-1	3020	2073	1280	3600**	4190

* Average of four separate cross-sections

** Discrepancy between theoretical and observed diameter is probably due to the slight polydispersity observed in this run.

corresponds very closely to the diameter found by electron microscope observation of the unsliced particles $D_{l\ expt}$.

B. Seeded Polymerizations 2: Autoradiography

We now consider two limitations inherent in the use of butadiene tagging and subsequent particle slicing as a means of physically observing the core-shell morphology. One could argue that the morphology revealed in our butadiene tracer work was caused by the incompatibility between the polystyrene molecules of the seed particle and the poly(styrene-co-butadiene) molecules of the second generation of growth. This problem was first discussed with reference to the experiment in which a run in progress was "spiked" with butadiene (4). In the work just described less than 0.7 wt-% butadiene was utilized and evidence of incompatibility was never observed. Although we had reason to conclude that incompatibility was not affecting our arguments, we felt it imperative to establish an insolubility free test.

A second limitation is imposed by the method used to obtain the ultrathin sections for viewing in the electron microscope. It was found, for the most part, that only isolated, single particles in the imbedding resin yield effectively to ultra-microtomy. In preparing the samples for slicing, we have been unable to effectively disperse the particles, and they tend to agglomerate in the embedding resin as illustrated in Figure 10. The knife merely scrapes over these agglomerates, and singly dispersed particles are

Figure 10

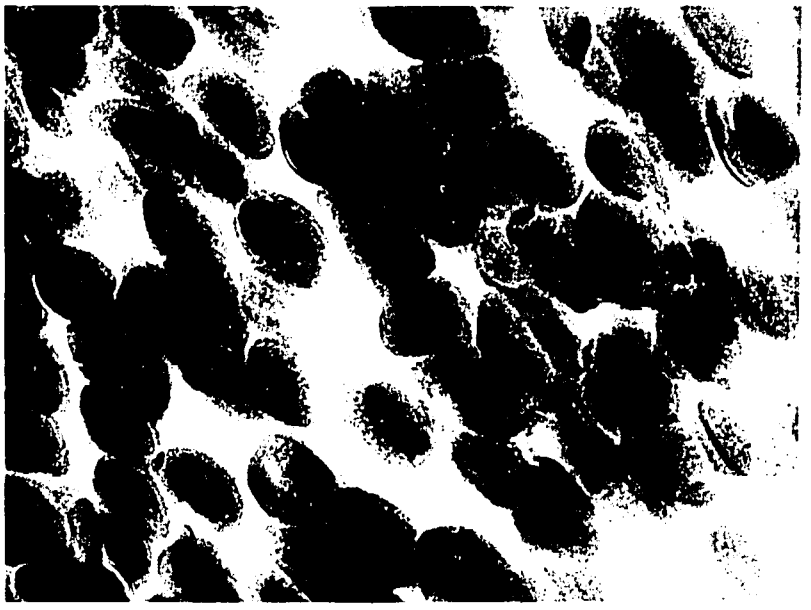

Field of imperfectly sliced latex particles distorted to elliptical shape (51,300X).

uncommon. Finding the confirming structures in the electron microscope is then akin to looking for the proverbial needle in the haystack. Consequently, this approach could not have a statistical basis.

To eliminate these limitations, plus any others one might associate with the butadiene tagging and slicing technique, we undertook a series of experiments that utilized tritiated styrene as the tagging agent and autoradiography as the detecting method. Tritiated styrene could never be argued to introduce compatibility problems, and the experiments were performed in such a way that slicing was not required and thousands of particles could be observed. Ordinarily, the technique involves the use of radioactive tracer elements which have been incorporated into a given sample. The location of the tagged molecule within a sample can be ascertained by coating microtomed slices with a fine grained photographic emulsion. The exposed silver grains in the photographic emulsion then determines the position of the tagged molecules in the sample when observed in the electron microscope. We employed a variation of the technique —— to be described in the next paragraph —— that eliminated the need to slice. In addition, the observation of slices would not be satifactory because the limit of resolution of an autoradiogram is —— at best, of the order of 500Å (6,35) —— certainly not good

enough for our purposes. The latter consideration imposed no limitation because of the procedures we employed.

Tritium is an emitter of low energy β-particles (maximum 18 Kev); these β-particles have a very low track length and many of them can be stopped in a material such as polystyrene (6). The essential experimental idea to verify the structure is depicted in Figure 11 and is described as follows: Prepare an active latex seed (polymer I) by incorporating tritiated styrene monomer in its synthesis. The seed was made radioactive to a specific activity of 0.05 mCi/mg to give about ten traces in about 62.5 days. The calculation is outlined in Appendix II. A photographic emulsion coating such a particle should show numerous traces (Figure 11a). Add fresh inactive monomer (monomer II) to the active seed to achieve equilibrium saturation and recommence the polymerization. If the core-shell morphology does not persist but active polymer I and inactive polymer II are uniformly distributed in the final product, the particles should still show numberous traces when coated with a photographic emulsion. On the other hand, if the core-shell structure persists, the particle should show greatly deminished traces if the shell of inactive polymer II is sufficiently thick (Figure 11b), since the efficiency of the photographic film is very sensitive to inert layers

Figure 11

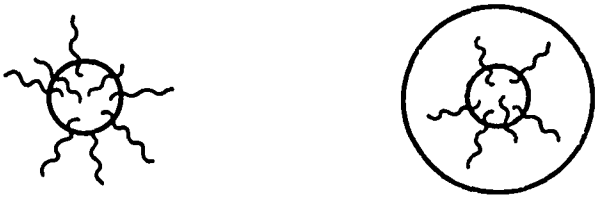

a. Uniform tagging

b. Tagged-core, untagged-shell

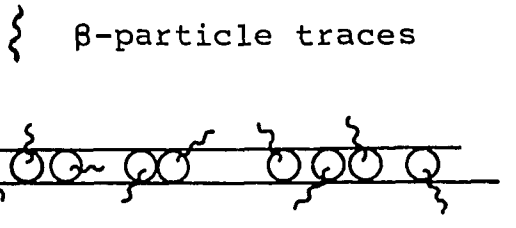

c. Latex particles between support film and photo-emulsion

Schematic showing the application of autoradiographic techniques to the study of latex particle morphology. (a) β-particles activate photo-emulsion. (b) β-particles are absorbed within untagged shell and photo-emulsion receives no exposures. (c) Latex particles sandwiched between parlodian film and photo-emulsion.

between it and the source. It is impossible to uniformly coat the particles with the photographic emulsion as depicted in Figures 11a and 11b. In practice the particles are placed on a parlodian-coated microscope grid in the conventional manner, and then a film of the photographic emulsion is placed over them as depicted in Figure 11c. In such a situation, not all the traces can be recorded. Nonetheless, the fraction of β-particles directed toward the photographic film should be the same from sample-to-sample and no biasing should be introduced with this technique.

Experimental

To execute this series of experiments we prepared the latex particles described in Table IV. They were synthesized with minor modifications, using the recipes of Woods et al.(19,31) and the procedures previously described. In order to conserve the precious active styrene, all polymerization runs were scaled down to 25 ml small glass reactors described in Appendix I. The tritiated styrene was obtained from New England Nuclear, Inc., Boston, Massachusetts with a specific activity of 0.5 mCi/mg at inhibitor concentration 12T. The active seeds contained 10% of this tritiated styrene. The latex in row 2 of Table IV was seeded once and that in row 3 was seeded twice.

Table IV

Latex Particles Used in Autoradiography Experiments

Type of particle	Where Tagged	Seed Diameter Å	Final Diameter Å	Shell Thickness Å
1. seed	throughout	1520	----	----
2. second generation	seed	1520	2620	550
3. third generation	seed	1520	4180	1330
4. seed	throughout	3410	----	----
5. seed	untagged	3230	----	----

The prepared latex specimens of Table IV were diluted with distilled water and applied to parlodian film supported on a copper electron microscope grids using standard techniques. The latex specimens on the parlodion film were first coated with a thin (ca. 100Å) layer of carbon (by vacuum deposition) and then with a monolayer of fine grained photographic emulsion, Ilford L4, (gel form) manufactured by Ilford, Ltd., Ilford, England. The thin carbon films serve to help stabilize the photo-emulsion. The photographic emulsion was applied by the "loop" method (36) described in detail by Stevens (37). In this method the fine grained photographic emulsion is melted and diluted to a free flowing liquid.

A metallic loop, much like a "bubble wand", is dipped into the diluted emulsion. The loop is withdrawn with a monolayer of emulsion across it, then allowed to dry to a film. When dried the film is placed over the copper grid containing the latex specimen. The photographic emulsion coated latex specimens are then stored in light tight containers which contain dry nitrogen and dessicant. The storage time to attain sufficient exposure of the photographic emulsion was greater than three weeks. Grids containing each kind of latex specimen were removed after 648 hours and 1608 hours, and developed using the methods of Stevens (37).

It was necessary to see if the silver halide particles uniformly coated the latex particles so proper contact could be obtained for β emission exposure of the photographic emulsion. Latex particles coated with photographic emulsion as described above were purposely exposed to white light and developed. The grids were then examined under a scanning electron microscope at 20,000X. Uncoated latex particles appear as smooth spheres, whereas latex particles coated with the emulsion appear rough and somewhat irregular. As can be observed in Figure 12, silver halide particles do indeed cling all over the latex particles. Additionally, as will be observed in subsequent autoradiograms, it is virtually impossible to focus properly on the latex particles when

Figure 12

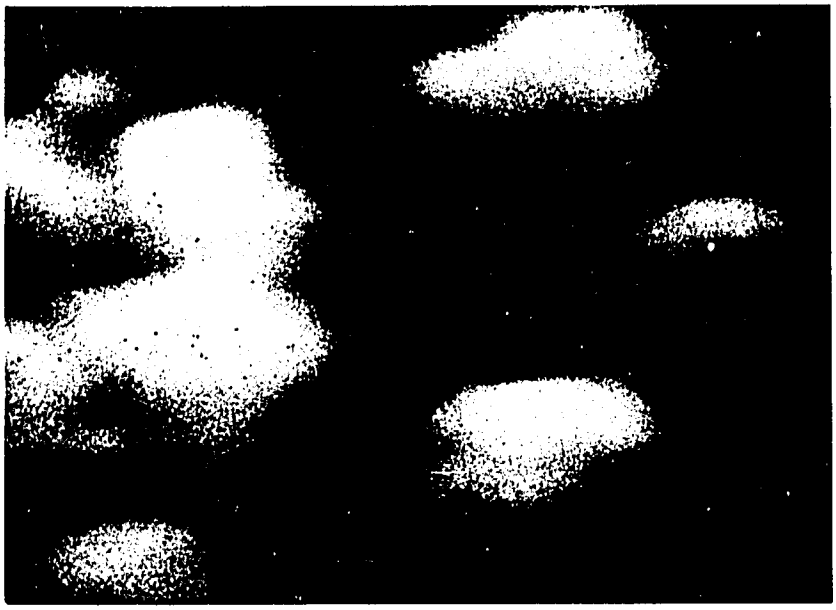

Scanning electron micrograph showing polystyrene latex particles coated with the autoradiographic photo-emulsion (20,000X).

they are properly blanketed by the photoemulsion. This inability to focus on the latex particles served as another check for proper photoemulsion coverage.

Results

In order to perform a valid autoradiographic analysis only areas of grids that contained latex particles smoothly coated with photographic emulsion were considered. An area of a grid that had either the parlodion support film or the photographic film torn away was not counted. An example of this sort is shown in Figure 13. On the other hand, some grid spaces showed considerable exposure of the photographic emulsion, as in Figure 14, but no latices. Figure 14 additionally illustrated the squiggly appearance of silver traces.* Observations of this kind were only found for the 1520Å tritiated latices. These findings were considered valid for analysis since in this case the parlodion film containing the active latices broke after exposure leaving only the exposed photographic film. In some instances, the supporting parlodion film was actually observed, while within the electron microscope, to tear and curl up on the copper grid taking the latices with it. Figure 15 shows a case where the parlodion film was observed to tear and curl and

* The triggered silver halide particles usually developed as a thread of silver. In some cases, the silver halide developed to silver keeping its shape. And in a few cases, the silver halide developed to an essentially round particle (see Figure 18).

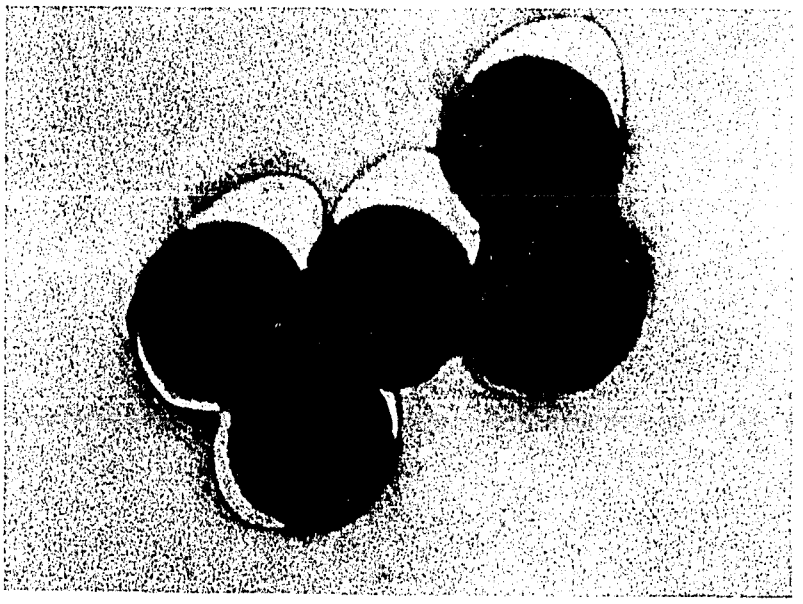

Figure 13. Electron micrograph of latex particle with torn film indicating possible loss of photographic emulsion. Such samples were not analyzed (56,430X).

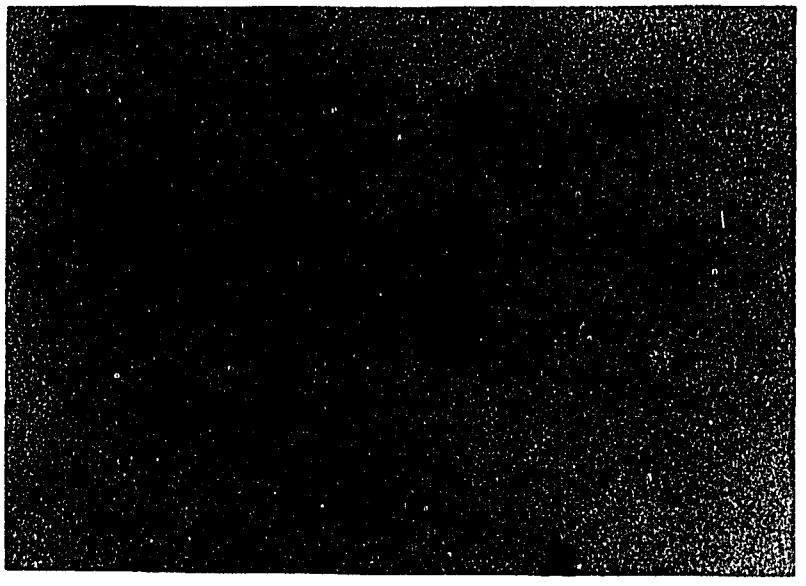

Figure 14. Electron micrographs of autoradiographic traces. This micrograph shows the strands of developed silver crystals due to the β emissions from the tritiated latex particles. The tritiated latex particles were observed to move from the grid space, due to the breakage of the parlodian support film after exposure. The latex particles are therefore not seen (25,050X).

eventually move the latices to the grid away from the silver halide particles they had previously exposed.

A progressive decrease of exposed silver halide particles was observed in going from the first generation tritiated core latex (sample 1) to the doubly seeded, third-generation latex (sample 3). The main results are displayed in Figure 16 (sample 1 of Table IV) and Figure 17 (sample 3). The very significant decrease in triggered silver halide particles in going from the first generation seed to the third generation latex is clearly evident. Sample 2, a second generation latex not shown, gave results between those of samples 1 and 3. The control samples 4 and 5 (Figures 18 and 19, respectively) are for comparison to a homogeneous active particle and for background, respectively. Samples 1 through 5 were identically photographically processed. The exposure time for these samples was 1608 hours. Another run was processed at 648 hours and gave essentially the same results. Upon counting exposures we have found that the decrease of silver halide exposures in going from the latex seed to the doubly seeded (third generation) latex was at least two orders of magnitude, with the exposure counts for the doubly seeded latex running just above background. This is shown in Table V. To insure that the photographic processing did not interfere with our findings,

Figure 15. Electron micrograph showing auto-radiographic traces caused by the tritiated seeds after movement of the seeds due to breakage of the parlodian support film under the electron microscope beam. This micrograph shows why traces may be a considerable distance from the active seeds. The active seeds can be seen near the copper grid (46,170X).

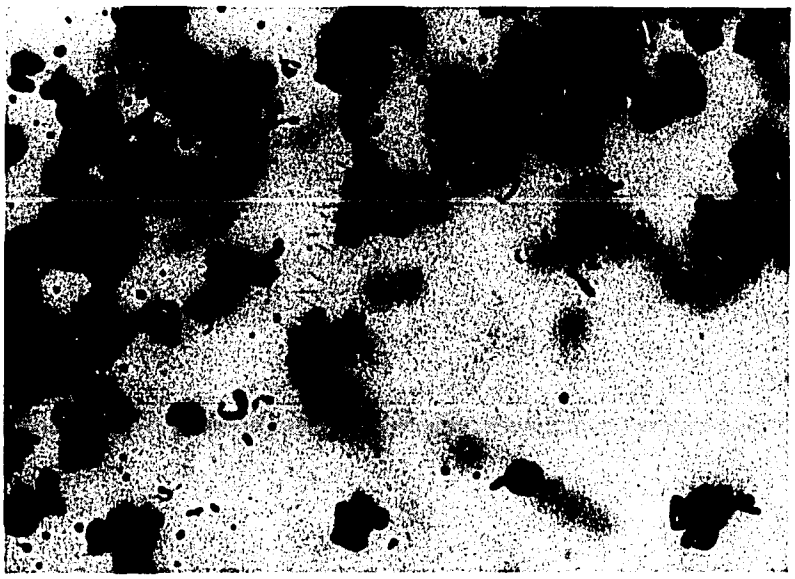

Figure 16. Autoradiograph of 1520A° seed latices with tagging throughout, showing very large amount of traces near the tritium active lattices. Exposure time: 1608 hours. The particles are observed as grey spheres in the background, while the traces appear as black irregular dots, strands and clusters (23,085X).

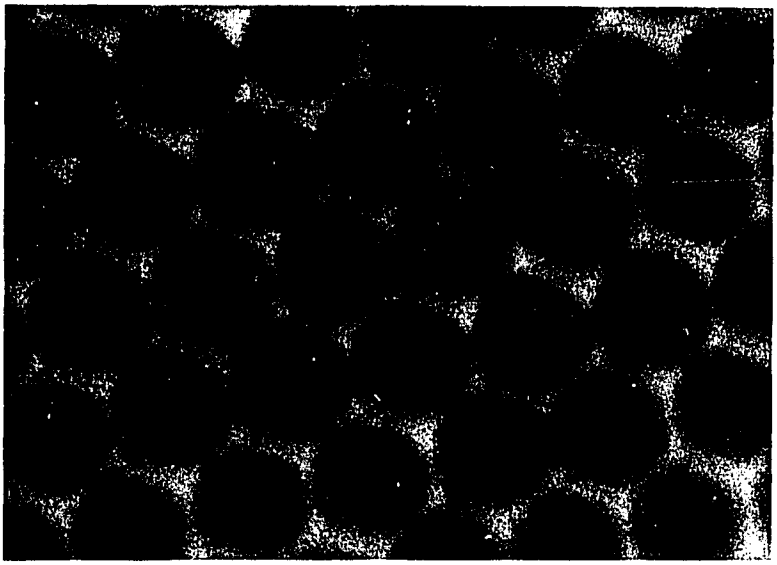

Figure 17. Autoradiograph of 1520A° seed latex with tagging throughout, twice encapsulated with pure poymer to 4180A°. Essentially no traces were observed in such samples. Exposure time: 1608 hours. The lattices shown here have distributed themselves in an hexagonal array (46,170X).

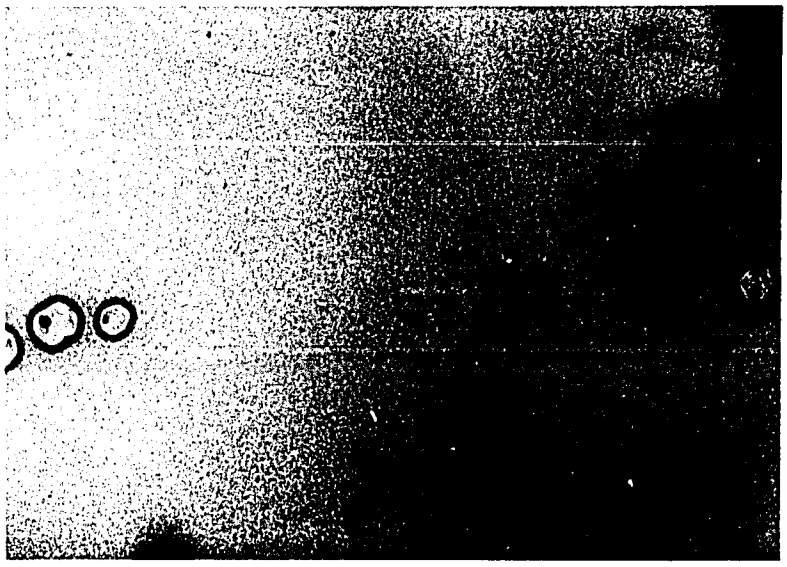

Figure 18. Autoradiograph of 3410A° seed control lattices with tritium tagging throughout, showing traces in the form of nearly spherical globules. Exposure time: 1608 hours. The latex particles are observed in the upper right hand corner (46,170X).

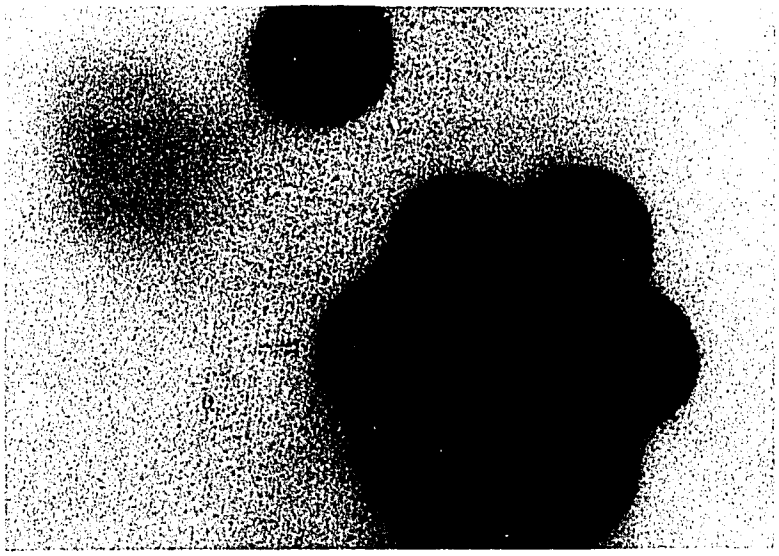

Figure 19. Autoradiograph of 3230A° seed control latex particles with no tritium tagging. This sample determined background where essentially no triggering was observed. Exposure time: 1608 hours. (56,430X).

Table V

Comparison of Recorded Radioactive Counts on Latex Particles Used in Autoradiography Experiments, 1608 Hours Exposure Time

Type of Particle	Where Tagged	Numbers of Fields Counted	Average Number of Particles in Field	Number of Counts Observed in Field
seed	throughout	20	200	>1000
third generation	seed	20	250	5
seed	throughout	15	100	325
seed	untagged*	20	300	4

* Control for background

by perhaps properly developing one set of specimens and not another, we processed the core samples (sample 1) and core samples with two shells (sample 3) on the same grid so they both would be treated identically. We again found, as shown in Figures 20 and 21, that most of the exposures occurred at or near the seed particles. In addition, the homogeneous tritiated latex particles (sample 4) gave more silver halide exposure than either of the second or third generation latices (samples 2 or 3) giving further evidence that the core-shell model prevails in these seeded, monomer-polymer compatible polymerizations.

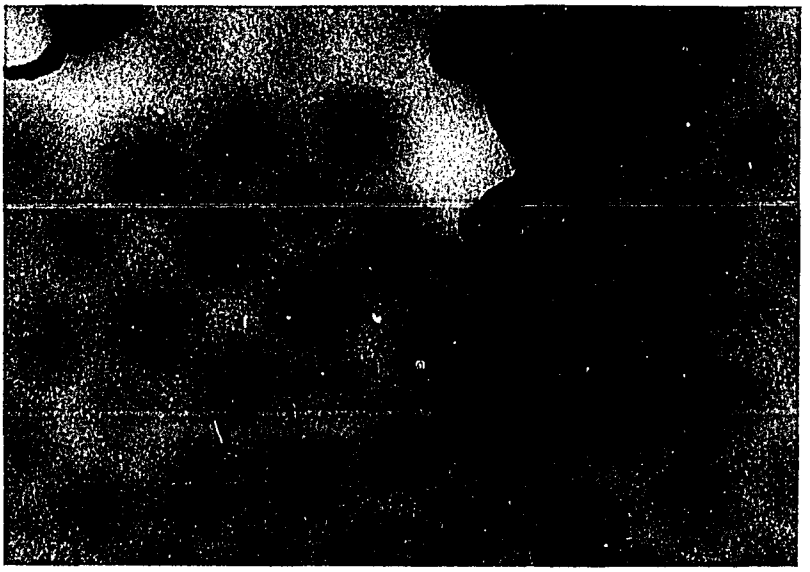

Figure 20. Detail of homogeneous active seed lattices of (sample 1) 1520A° from the mixed grid (samples 1 and 3) showing autoradiographic traces (87,750X).

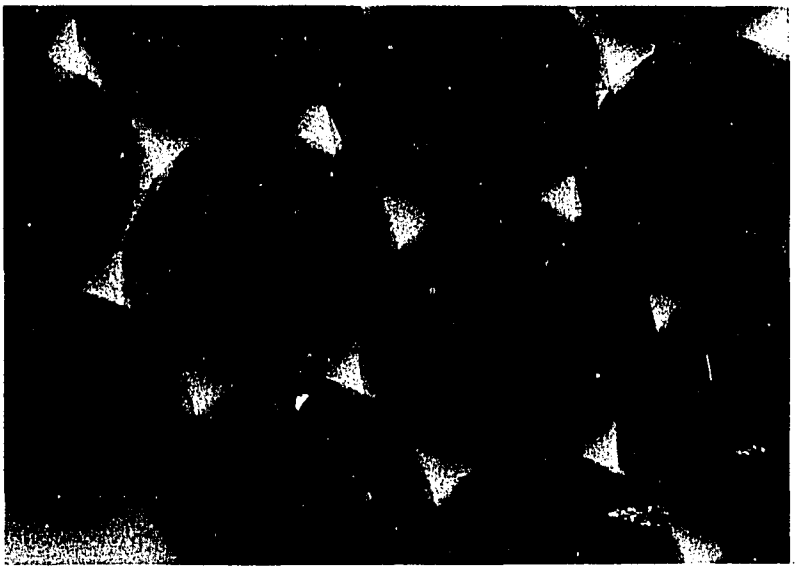

Figure 21. Detail of the 4180A° twice encapsulated latex from the mixed grid (samples 1 and 3) showing essentially no traces (87,750X).

C. Interpretation of Seeded Polymerization Experiments

To reiterate: The most important feature of the afore-described seeded polymerizations was that they were initiated with the latexes in a state of equilibrium saturation with monomer. Furthermore, the core-shell morphology was observed to prevail in the final product for which the first generation seed polymer (polymer I) was fully compatible with both the charged monomer (monomer II) and the second generation polymer obtained therefrom (polymer II). Since the core diameters closely corresponded to the seed particle diameters and since there was no evidence of appreciable polymer I - polymer II interpenetration between the core and shell, it appears that the major portion of polymer II is located within the shell of the second generation latex particle.

It now remains to develop an explanation for the experimental facts just summarized. First, it is clear that a diffusion controlled kinetic mechanism is not supported by the experimental results. We should also keep in mind the additional fact that, according to the studies of van den Hul and Vanderhoff (10) as well as Ottewill (11), with persulfate initiation the major portion of sulfate end groups remain on the surface of the particles——even through successive generations of seeded polymerizations.

This means that nearly all the polymer molecules are bound to the particle-water interface by their chain ends.

We would now like to consider two possible explanations for the formation of the core-shell morphology. In the first, one could postulate that the monomer and polymer are uniformly distributed at equilibrium; upon reinitiation, each second generation polymer chain is bound to the swollen particle surface and must grow there; monomer II, which swells the entire network, migrates toward the periphery as the supply there diminishes. As monomer II migrates to the surface, it must displace polymer I chain segments toward the center. Hence, as polymerization proceeds polymer I chain segments collect at the center and polymer II segments collect in the peripheral region, thereby forming a core-shell structure. A difficulty with the latter mechanism, especially as the conversion of monomer II progresses, is that it requires extensive diffusion of polymer I chains through the polymer II chains. The most serious difficulties are (i) that it requires the preferential migration of polymer I chains over polymer II chains; and, from a diffusional point of view, polymer I chains are indistinguishable from polymer II chains, and (ii) as we show in Section V the self-diffusion of high polymer molecules is so slow that diffusive separation would be negligible.

In an alternative explanation, one could postulate that monomer II does not uniformly swell polymer I but that a major portion of it collects in the peripheral region of the particle, i.e., encapsulation occurs. Upon reinitiation, monomer II converts to polymer II in the peripheral region, thus forming a core-shell structure. Any monomer II that might be located in the central region of the swollen particle would migrate to the peripheral region as the monomer located at the periphery was consumed.

The first mechanism is based upon the fact that the locus of polymer chain ends is the particle-water interface. The second is based upon the supposition that monomer II is located in the peripheral region at equilibrium saturation before the second generation polymerization is initiated. The latter is in accord with our earlier proposed core-shell model for a growing latex particle (4). An experiment was devised to differentiate between the two foregoing explanations: First deionize the seed latex, by diluting with distilled water and amberlite MB3 mixed bed ion exchange resin*, to remove residual initiator (49). Prepare the seeded charge, taking

---

* Product of Rohm and Haas Company

care to replace the soap lost in the deionizing process. Add trace amounts of butadiene, as before, with the monomer II. Utilize the oil-soluble initiator, benzoyl peroxide (0.1 wt-% based on monomer II) and recommence polymerization. The question is: Does the monomer distribute uniformly as per the first explanation or does it tend to locate in the peripheral region of the particle as per the second explanation? Now, before repolymerization, the benzoyl peroxide should distribute essentially throughout the particle in direct proportion to monomer II; furthermore, polymer II chains will not be attached to the particle surface. Hence, if uniform distribution of monomer II prevails, polymer II should be uniformly distributed throughout the final latex particle and no core-shell morphology should be observed. On the other hand, if monomer II tends to concentrate near the particle periphery, then a core-shell morphology should be observed in the final particle.

We did indeed execute the foregoing experiment. As shown in Figure 22, the core-shell morphology is clearly evident. In this case the core diameter (2440Å) observed by electron microscopy does not correspond to the seed diameter (1640Å). The difference is in all likelihood due

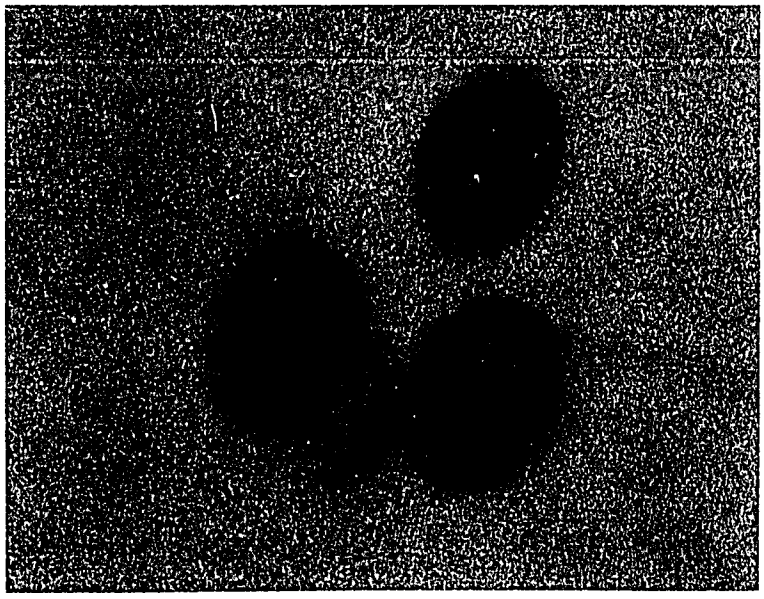

Figure 22. Ultra-thin cross-section of a latex particle prepared in a seeded emulsion polymerization, showing the core-shell morphology. The second stage of growth was initiated with the oil soluble benzoyl peroxide initiator after the monomer II charge had achieved equilibrium saturation with the polymer I seed. Core/shell diameters : 2440A°/2750A° (114,750X).

to some monomer reacting in the core. This is plausible for in this experiment the oil soluble initiator is not constrained near the surface as is the persulfate initiator. Nonetheless, the result shown in Figure 22 strongly supports the notion that, at equilibrium saturation, monomer and polymer are not uniformly distributed but that there is a high concentration of monomer near the periphery of the swollen latex particle.

In summary, with monomer (or solvent) and seed latex at equilibrium saturation, we propose that the polymer and monomer are not distributed uniformly but that a major portion of the monomer actually encapsulates the swollen seed particle. Furthermore, the particle morphology appears to be controlled by molecular-thermodynamic factors. We consider the latter in Section IV.

D. Range of Applicability

We next sought to delineate the range of conditions over which the core-shell morphology prevailed. The parameters studied were: (i) butadiene concentration in monomer II, (ii) seed particle size, and (iii) seed molecular weight.

1. Incompatibility Effects —— Butadiene Concentration Variation in the Shell

As an adjunct to the equilibrium encapsulation studies we have explored the effect of increasing the butadiene to styrene ratio in the monomer II charge for a polystyrene seed on the particle morphology. This situation falls into the general category of overcoating with a monomer system which is substantially soluble in the polymer seed but the second generation polymer is incompatible with polymer I. Note that in this series of studies we were seeking to enhance incompatibility between polymers I and II rather than suppress it as we had in all our earlier studies. Thus, we were seeking to ascertain the role of polymer-polymer compatibility in controlling latex particle morphology.

Polymerizations

All latexes were prepared by following the formulations and procedures of Woods et al. with some slight modifications. The formulations are tabulated in Table VI below.

Table VI

Formulations for Butadiene Concentration Variation in the Shell

Ingredients	Seed Preparations	Seeded Polymer-izations
Water	172.74 gm	172.98 gm
Monomer	122.52 (styrene)	62.33 (styrene and butadiene)
Siponate DS-10	0.219	none
Triton X-100	4.233	0.334
$K_2S_2O_8$	0.225	0.037
NaOH	0.420	0.0051
Seed charge	none	64.29
Dodecanemercaptan	none	3.0

The polystyrene seed particles (as determined by electron microscopy) were 1840Å in diameter. In the reseeding experiments the monomer to polymer ration was 2.4 (just below saturation), and 48 hours were allowed for equilibration of monomer and polymer. The measured final particle diameter was 2740Å versus a value of 2760Å calculated from the formulation stoichiometry and the seed diameter of 1840Å. The butadiene concentration in the overcoat was varied as 6, 10, 15, and 50 wt-% based on monomer II charge. For the charge containing 50 % butadiene, the reaction time increased to 36 hours from the normal 10 to 12 hours for an all styrene charge. The

butadiene was obtained by distillation from a pressurized cylinder, with cooling coils immersed in an acetone-dry ice bath.

The electron microscope techniques for direct observation of latex particles are standard. The procedures for imbedding, slicing, and staining are described in References 32-34. The particles containing 50% butadiene in the monomer II charge were fixed with osmium tetroxide prior to destabilizing and subsequent imbedding.

Observations

The essential features of the core-shell morphology first displayed in these studies (Figure 6) prevailed in all the micrographs observed. In all cases the core and shell dimensions correspond to the original seed and final diameters, respectively. Figures 23a to 23d show thin cross-sections obtained for increasing butadiene content. The most pronounced morphological changes which appear with increasing butadiene content are best displayed in Figure 23b for the 10% butadiene formulation. Two features are noteworthy: (i) the occurrence of a dark ring around the core and (ii) dark spots inside the core, both of which indicate a high concentration of butadiene. Close examination of the shells in these micrographs shows that the dark ring at the periphery of the core gradually loses its intensity toward the outer edge of the particle. This result is an indication

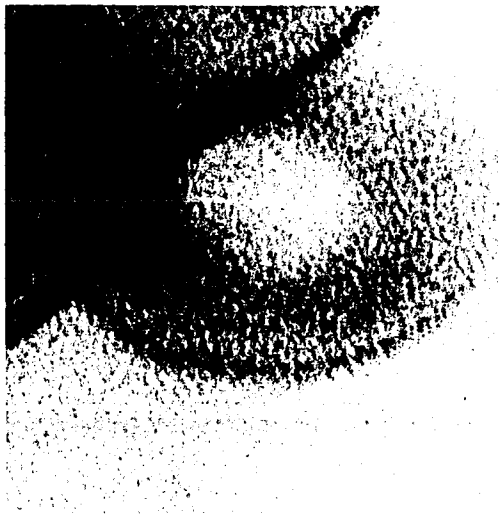

Figure 23a. 6% butadiene in monomer II charge (249,230X).

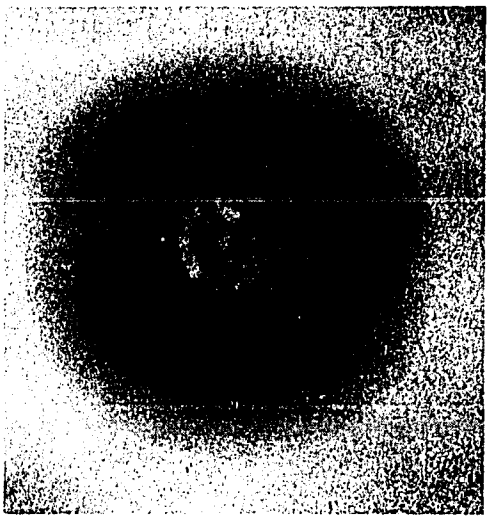

Figure 23 b. 10% butadiene in monomer II charge (205,200X).

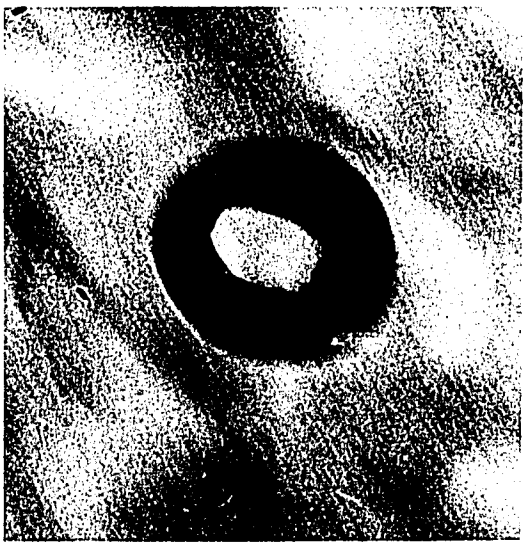

Figure 23 c. 15% butadiene in monomer II charge (213,360X).

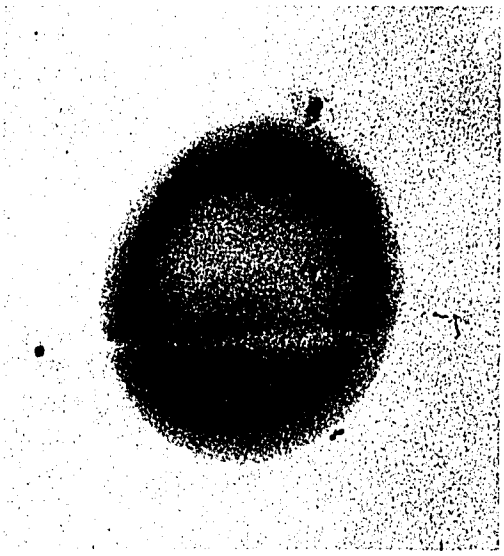

Figure 23 d. 50% butadiene in monomer II charge (139,650X).

Figure 23. Ultra-thin cross-sections of latex particles prepared in two stage emulsion polymerizations. Seed growths were conducted under conditions of equilibrium saturation with varying amounts of butadiene in the monomer II charge.

that the butadiene added with monomer II tended to react first, probably because of the addition of the mercaptan promoter. In any event, there appears to be a gradient in the butadiene repeat unit concentration.

These micrographs provide additional evidence supporting the core-shell morphology. If the system had reacted homogeneously after equilibration of the seed and added monomers, the morphology should have appeared similar to a blend of incompatible polymers with small regularly dispersed domains of poly(styrene-co-butadiene) in a continuous matrix of polystyrene as depicted schematically in Figure 24. In any event a layered gradient would not be the likely result of a homogeneous polymerization.

Under electron microscope observation the inclusions within the core were actually observed to move about in a rather rapid random motion. This motion has been tentatively ascribed to differential heating of the sample area by the electron beam. Figure 25 shows an uncommon micrograph of a field of thin sections for the 10% butadiene specimen of Figure 23b.

The observation of butadiene in the core is evidence that some polymerization occurs within the core —— most likely a modest amount in light of the original arguments leading to the core-shell structure (4). Some caution ought to be followed, however, in extrapolating an interpretation based

Figure 24

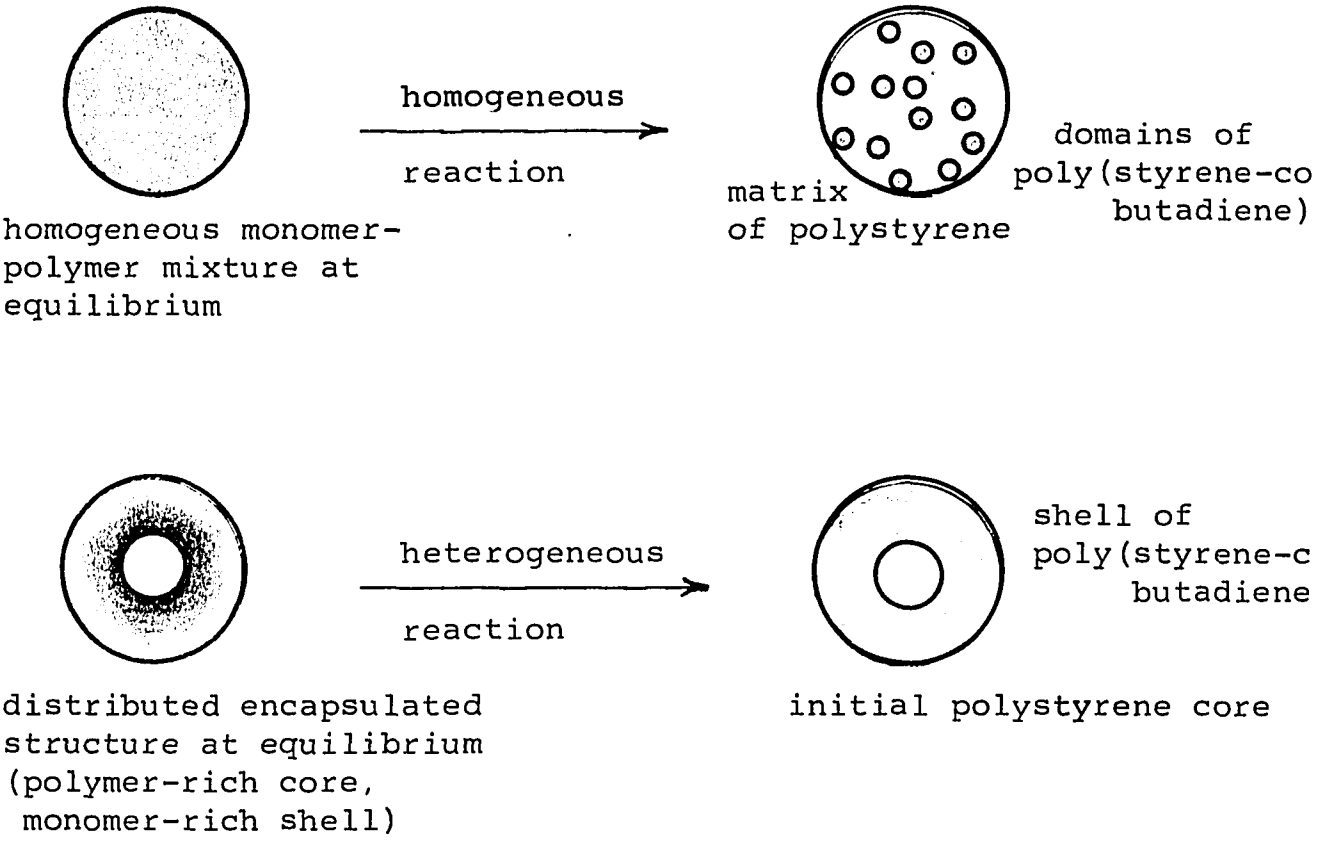

Comparison of final morphological features of homogeneously reacted swollen latex to heterogeneously reacted latex

Figure 25

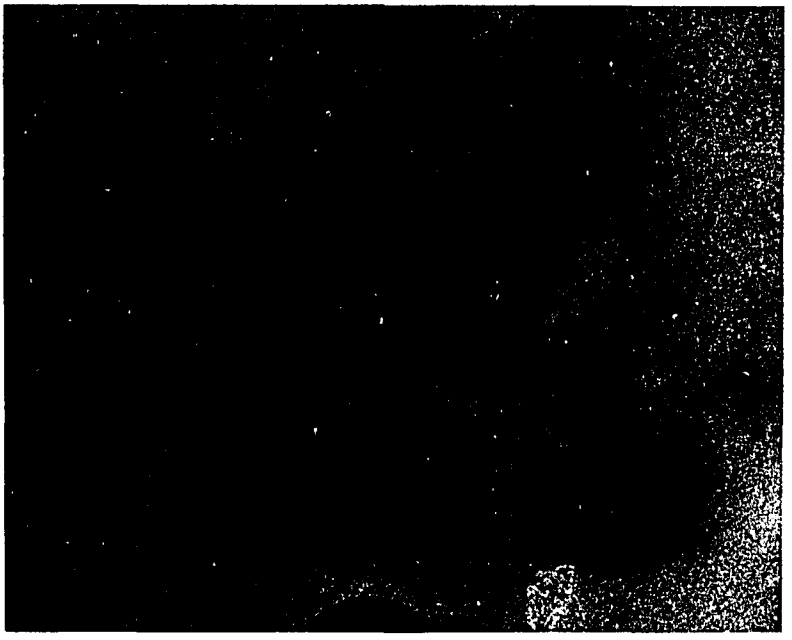

A field of cross-sections obtained from the latex sample containing 10% butadiene in the monomer II charge (129,675X).

on micrographs obtained from latexes at 100% conversion to a kinetic situation that prevails from zero to 60% conversion. [Shortstopping the reaction at lower conversions to obtain the requisite samples for microscopy does not offer an alternate solution because of the shrinkage (and therefore, changes in morphology) such particles would suffer when unreacted monomer was removed].

Figure 26 is a micrograph of a platinum shadowed 50% butadiene latex particle (not sliced but deposited on a collodion film in the normal manner). The core-shell morphology can be clearly discerned becaused of the difference in electron opacity between the rigid polystyrene core and the flattened copolymer shell. Curiously, as shown in Figure 23d, the 50% butadiene thin section does not show the core inclusions as observed in Figure 23b for the 10% butadiene specimen.

The only analogous study of ultra-thin sections we know of is reported by Kato (38) for ABS* latexes. He varied the ratio of rubber seed (polybutadiene) to glassy-shell (copolymer of acrylonitrile and styrene) from 80/20 to 20/80 (he did not specify the acrylonitrile/styrene ratio). He also varied the rubber seed size. It is difficult to compare our results with his because he did not adequately describe the preparation procedures in the seeded polymerization, and

---

* A copolymer of acrylonitrile-styrene on a polybutadiene seed.

Figure 26

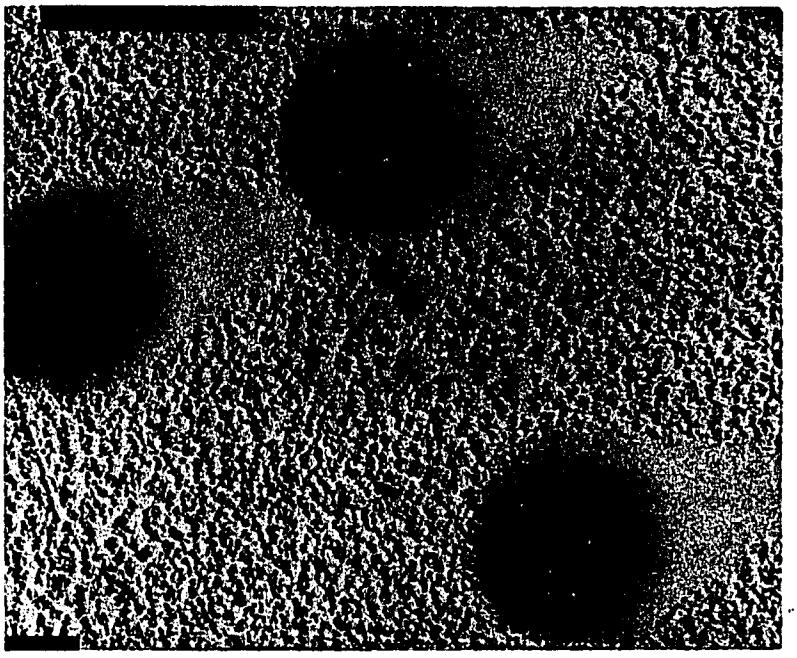

Micrograph of a platinum shadowed sample of latex containing 50% butadiene in the monomer II charge (57,710X).

the experimental variables in the seeded polymerizations were not the same. One of Kato's primary objectives was to demonstrate that the comonomer charge actually grafted in such a way to form a core-shell structure. He was evidently concerned with the effect incompatibility would have on the bonding between polybutadiene core and the newly formed acrylonitrile-styrene copolymer.

Kato found the core-shell morphology to prevail over a monomer II to seed weight ratio range of 0.25 to 4.0, the shell thickness increasing with increasing monomer II content. He also found that, when large and small seed particles were used together, the simple core-shell morphology prevailed only in the small particles. With the large particles (approaching 1μ in diameter after seeded polymerizations) copolymer II adhered to the surface in hemispherical, wart-like appendages, whereas we found the completely spherical core-shell morphology to prevail in particles up to at least 6500Å in diameter. It is impossible to explain the latter results with the scant polymerization procedures given by Kato; it might have resulted from a failure to allow sufficient time for latex saturation (see Bradford and Vanderhoff, Reference 39). Kato's micrographs also show inclusions in the core, indicating the presence of the second monomer as we have also noted. In the ABS system, the inclusions are more clearly

defined than they are in this work. It is impossible to unambiguously state the reasons for this without having more knowledge of Kato's formulations. It might possibly be ascribed to the different order of butadiene addition or to the fact that the seeds in Kato's work might be crosslinked, thereby enhancing phase separation of the included material. The role of these core inclusions in establishing a polymer's mechanical properties remains to be elucidated.

2. Particle Size

The prevalence of the core-shell structure for latex particles of diameter greater than 2000Å was established by our standard saturation seed polymerizations coupled with slicing, osmium tetroxide staining and electron microscope observation. Since formulations to produce small seed latexes (< 500Å) were not available, we returned to the original dynamic method first employed by Grancio and Williams (4,5). Growing latexes were spiked soon after nucleation with trace amounts of butadiene. The prevalence of the core-shell mode of growth at small particle diameters is clearly manifested in Figure 27. This micrograph shows a cross-section for a particle having a core diameter of about 650Å. The smallest core yet observed was 500Å. The largest core-shell particle observed in this series of

Figure 27

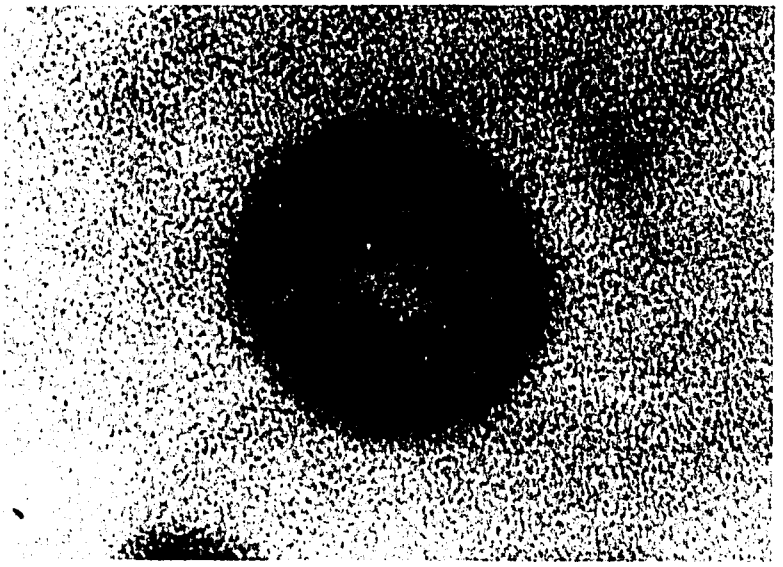

Typical (off-center) cross-section of one of the smallest core-shell particles observed. The run was spiked with a trace of butadiene just after nucleation. Core/shell diameters : 640A°/1320A° (282,150X).

experiments was 6500Å in diameter. See Table VII for other sized latexes for which the core-shell morphology was displayed.

In the synthesis of high molecular weight latex seeds, to be described in our molecular weight studies in the following section, small numbers of very large latex seeds (>2μ) were produced accidentally along with the primary monodisperse particles of 2560Å. (Such "accidents" are common in latex work. In this instance the generation of these large particles might be ascribed to the agglomeration of high molecular weight particles which tend to be unstable because of reduced amount of persulfate chain-ends on the particle surface). These large particles—>2μ—were included in a subsequent seeded saturation polymerization; and, as shown in Figure 28, they also exhibited peripheral growth. Since the saturation content of these large particles was not determined to predict shell thickness, we present these observations only as tentative evidence that peripheral growth can prevail even in a system approaching macroscopic dimensions.

Table VII

List of Latices of Various Sizes Showing Core-Shell Morphology

	Run	Core Diameter Å	Shell Diameter Å	Location of Stain	Method of Synthesis
1	1-23-2	640	1320	shell	dynamic
2	———	590	2000	shell	dynamic (4
3	1-12-1	1930	3070	core	equilibriu
4	1-27-1	2830	3120	core and outer shell*	equilibriu
5	1-33-1	5325	6500	shell	equilibriu

* Twice encapsulated run, with core and outer shell stained. See Figure 9.

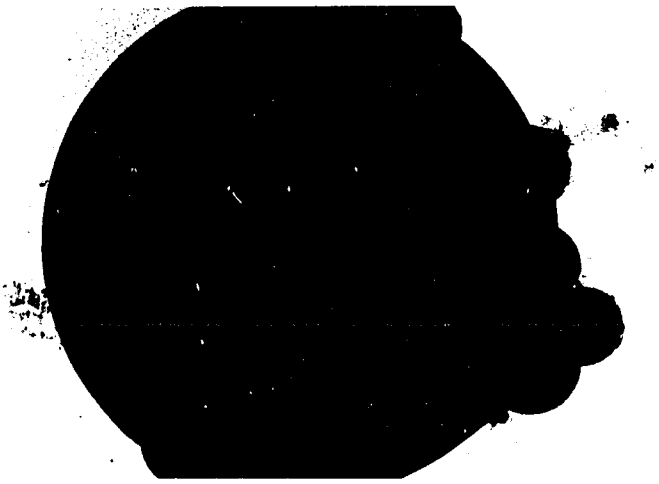

a. Micrograph of a whole particle (12,540X).

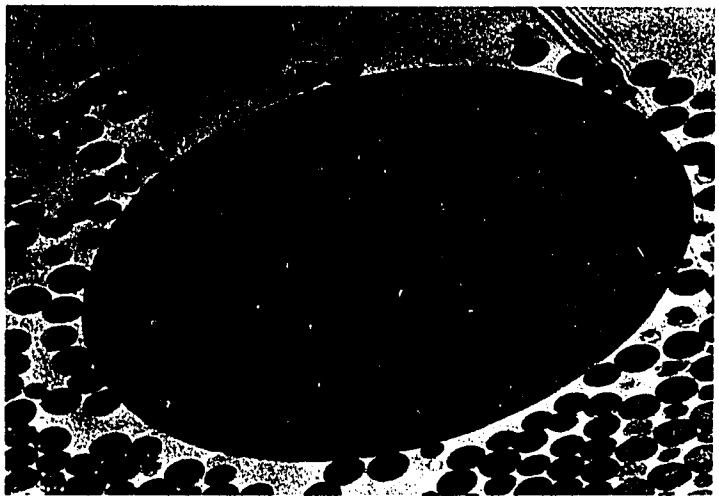

b. Ultra-thin section of large particle showing core-shell growth (28,215X).

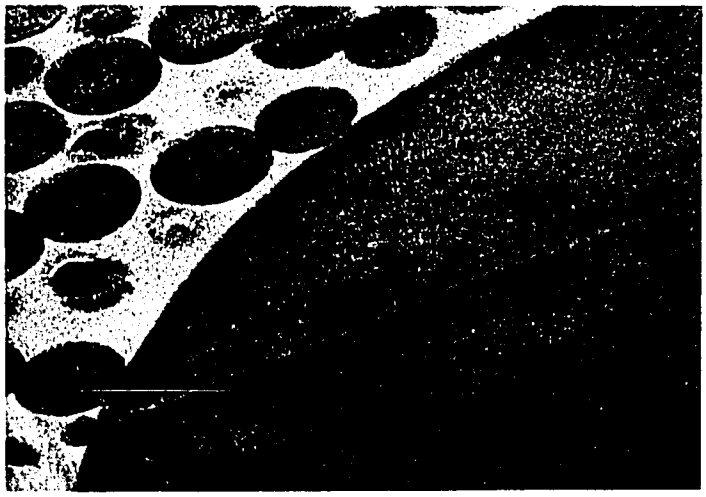

c. Detail of the surface of the large particle (53,625X).

Figure 28. Electron micrograph of the largest particle exhibiting core-shell behavior.

3. Molecular Weight

Latex seeds were synthesized in the size range of ca. 2000Å using the standard formulation, with the following modifications to vary molecular weight. Low molecular weight latexes were synthesized using the chain transfer agent dodecanemercaptan. Up to 3 wt-% (based on monomer) was added at the start. To obtain the high molecular weight latex only 18% of the standard quantity of initiator was initially charged. The viscosity average molecular weights of the various latexes were determined by standard viscometric procedures (40).

The equilibrium monomer saturation content of the various molecular weight latexes were determined by centrifugation in the manner previously described (see page 28) so as to determine the amount of monomer II required to saturate seed polymer I before repolymerization. The determination of the equilibrium saturation content of the monodisperse latexes is also of general importance since little work has been performed to determine these values; also accurate values of latex size, molecular weight and equilibrium saturation are necessary to validate any thermodynamic arguments concerning the swelling of latexes.

The results of the saturation experiments are presented in Table VIII. Note that equilibrium saturation tends to

Table VIII

Equilibrium Saturation Content of Styrene in Polystyrene Latexes of Given Molecular Weight at Particle Sizes Near 2000Å

Run	D_o Å	$\bar{M}_v$ x10^6	$[M]_w$ x10^6
1-61-1	1675	0.021	0.60
1-59-1	2290	0.659	0.65
1-56-1	1955	2.585	0.74
1-56-2	1850	2.638	0.73
1-52-1	2560	9.915	0.71

D_o - Seed diameter

$\bar{M}_v$ - Viscosity average molecular weight

$[M]_w$ - Saturation weight fraction of monomer in seed

increase with molecular weight. Since we did not work with the same size latexes for each molecular weight, we assumed that the influence of particle size is weak. From the limited data in the literature, we believe this assumption to be valid (41,42).

With the equilibrium saturation values established, equilibrium saturation repolymerizations were run to determine morphology. The standard microtoming and staining procedures were employed preparatory to electron microscope observation. The results are presented in Figure 29 where it is seen that the core-shell morphology prevails over the range of molecular weights studied —— from about 10^4 to 10^7.

Figure 29

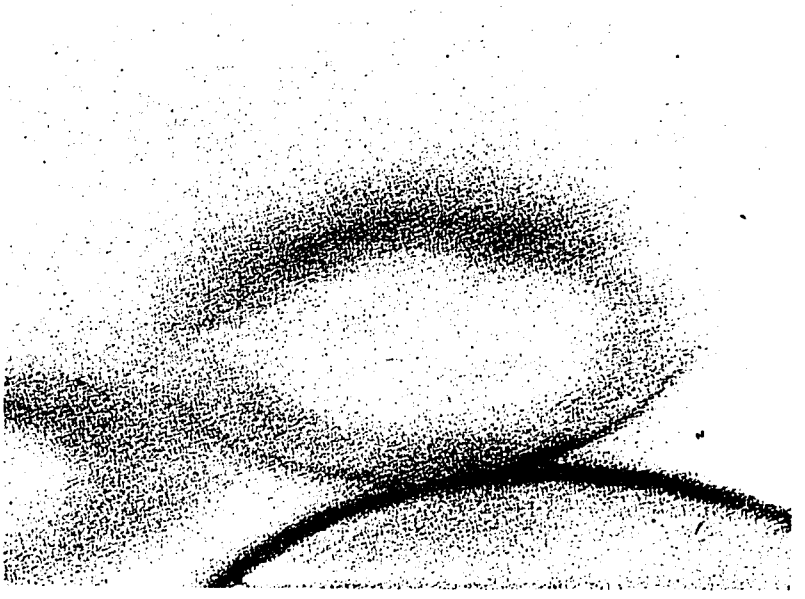

Figure 29a. High molecular weight core, $\bar{M}_v = 9.92 \times 10^6$, (205,200X).

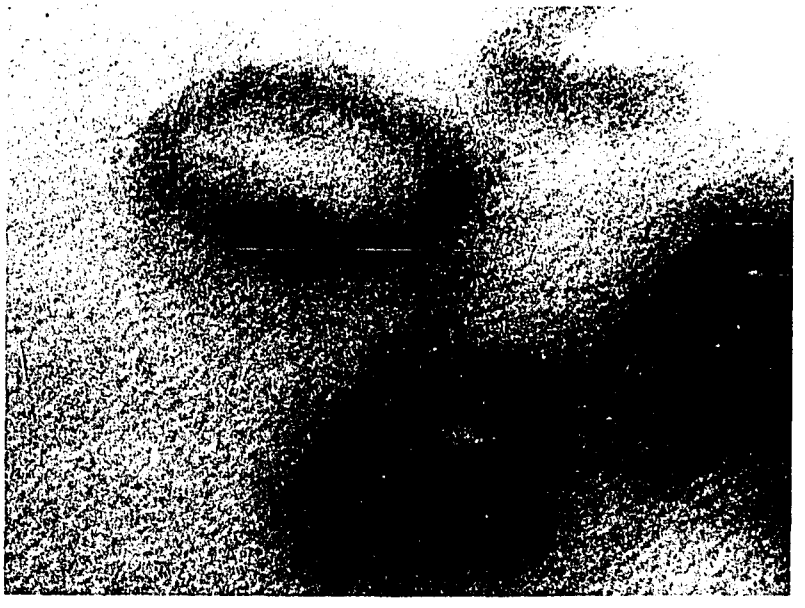

Figure 29b. Low molecular weight core, $\bar{M}_v = 0.021 \times 10^6$, (180,720X).

Electron micrographs of ultramicrotomed two stage latex particles with seed polymer I of high and low molecular weight.

E. Technological Implications

An area of major technological importance involves the wide-spread use of overcoating to modify polymers produced via emulsion polymerization. In this scheme polymer I in latex form is modified by the addition of monomer II. We show that the factors governing the core-shell mode of growth determines latex overcoating rather than controlled monomer addition or polymer I-polymer II incompatibility.

Overcoating

We now wish to discuss the implications of our findings with regard to the factors controlling the morphology of latex particles prepared in multistaged monomer additions. In macroscopic heterogeneous polymer systems, several factors control the morphology. Among these are the organo-chemical structure, the macromolecular structure, mixing (especially if the specimens are prepared from the melt), and orientation. In latex systems, the morphology is controlled by the organo-chemical structure, the macromolecular structure and, most importantly, by the mode of monomer addition. Bradford and Vanderhoff (39) have shown that the exterior morphology can be distorted from spherical in seeded polymerizations by not allowing sufficient time for the second stage monomer to saturate the seed particles. Similar effects were observed in competitive growth polymerizations where the monomer is

a poor solvent for the seed polymer. We are concerned with situations in which a spherical particle shape is maintained.

In practice, execution of the overcoating process is accomplished by adding the monomers in such a manner that they do not have sufficient time to completely "swell" the particle, and they tend to layer around the original seed particle to form a core-shell structure. Polymer-polymer incompatibility is thought to aid this layering process. The evidence presented in this dissertation suggests that one need not worry about diffusion or even incompatibility in compatible monomer-polymer systems; for, even under conditions of equilibrium saturation, core-shell structures can be obtained. This observation should ease the rigor of scheduled monomer additions in multi-stage latex synthesis.

This last contention is supported by the results obtained by Sperling et al. (43) who studied the dynamic mechanical properties of two-stage latex polymers prepared both by dropwise addition of monomer II to polymer I and by charging the total amount of monomer II all at once to polymer I. The polymer composition in both cases was 1:3 ethyl methacrylate to n-butyl methacrylate, each crosslinked with 0.4 wt-% tetraethyleneglycol dimethacrylate, corresponding to core and shell, respectively. Their data, summarized in Figure 30 are nearly identical for both specimens, thereby indicating

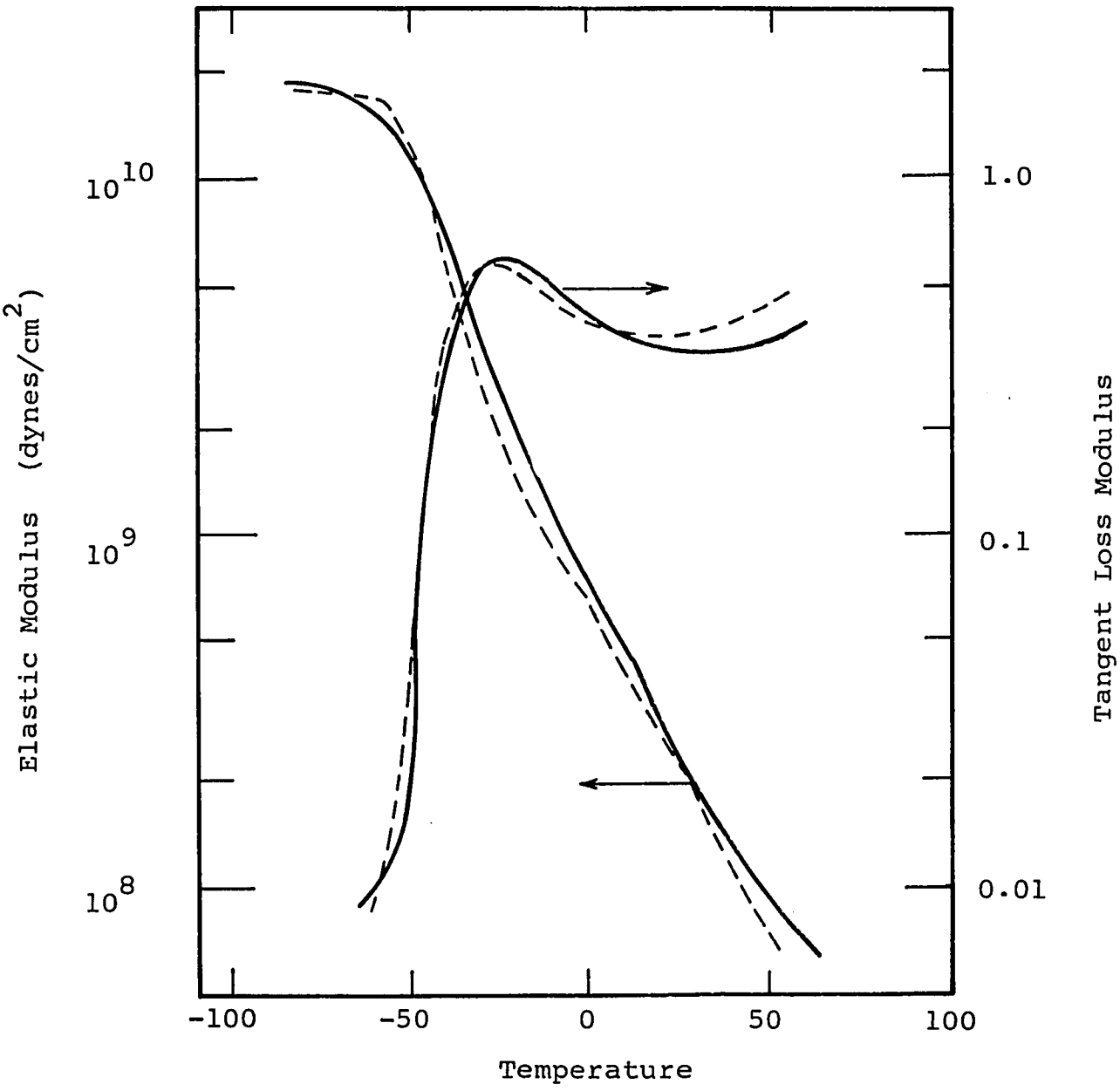

Figure 30. Dynamic mechanical behavior of latex prepared in a two-stage emulsion polymerization. Seed: one part PEMA. Overcoat: 3 parts PnBA. Polymerization temperature: 60° C. Monomer II Addition : ---- Dropwise. ——— All at once. After Sperling et al. (43).

that there are no important differences in the morphology of the two specimens.*

In order to ascertain how the inherent incompatibility of the component polymers might affect particle morphology, we prepared for electron microscope observation thin films of latex polymer. A thin film of the 10% butadiene latex polymer (Figure 31) was prepared by casting over water from a 1% amyl acetate solution. Grids were placed on the floating film and then picked up in such a way as to carry off the cast film. The specimens were dried and exposed to osmium tetroxide. The important point in this experiment is that we prepared this film from macroscopic homogeneous solution under conditions where the components were mobile and well mixed. The film observed should then pertain to the state of thermodynamic equilibrium and the structure observed in Figure 31 should also be independent of any mixing considerations as they are in incompatible styrene-butadiene systems prepared from the melt. Thus in seeded polymerizations where monomer II and polymer I are compatible, if the monomer actually swelled the seed particles uniformly and if incompatibility controlled the particle morphology, then structures similar to that shown in Figure 24a should be observed rather than the core-shell structure. In conclusion, for seeded polymerizations with compatible monomer-polymer systems, the incompatibility of polymer I with polymer II

*Slow monomer addition may still be required in order to maintain adequate temperature control.

Figure 31

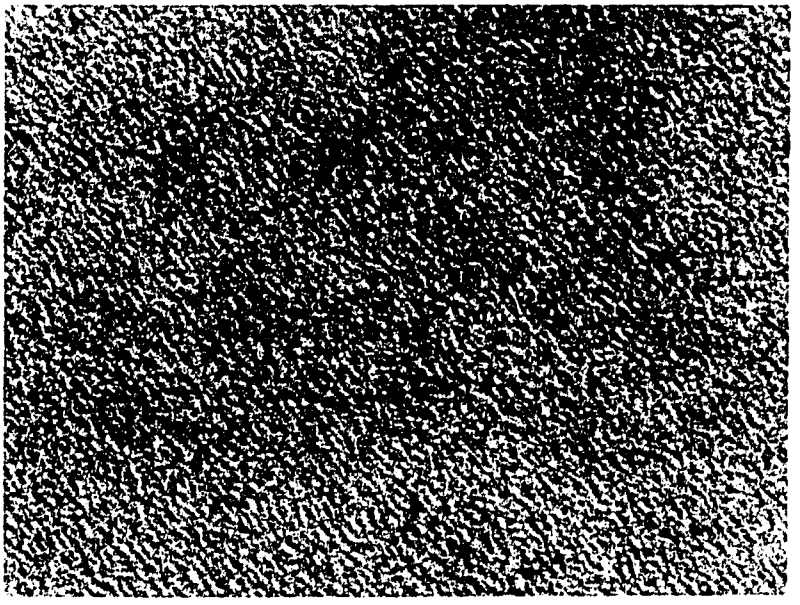

A thin film cast from homogeneous solution of the latex polymer containing 10% butadiene in the monomer II charge (407,550X).

is probably not a factor in controlling the primary features of particle morphology, and the dominating factor is the encapsulation phenomenon. Polymer-polymer incompatibility might very well be a controlling factor in establishing such secondary morphological features of the high butadiene content latexes as the butadiene inclusions in the core.

IV. THEORETICAL CONSIDERATIONS

Theoretical arguments are now presented to show that a segment density distribution of the type described is more likely than a uniformly distributed system. From a phenomenological point of view, a concentration gradient is always expected at the interface of a two component system. This notion was formalized by Gibbs. With the details of the gradient unknown, Gibbs related the surface excess (or deficiency) of one component to activity and interfacial tension by

$$d\gamma = - \Gamma_1 d\mu_1 - \Gamma_2 d\mu_2 \qquad \text{(Ref. 44)} \qquad (4)$$

where μ_1 and μ_2 are the chemical potentials, γ the interfacial tension and Γ_1 and Γ_2 are the surface excesses or deficiencies of the various components expressed in moles per area. In the case of latexes which contain monomer or solvent one is treating a microscopic environment where there is a high surface to volume ratio. For this reason, one cannot extrapolate thermodynamic data based upon a bulk (macroscopic) system which ignores interfacial effects to that of the microscopic latex environment. It follows therefore that one is not justified in assuming, a priori, that monomer and polymer (such as styrene, and polystyrene) are uniformly distributed in a latex environment simply because they are

mutually soluble in all proportions in a bulk situation.

In advance of more formal arguments, we now present a heuristic argument, based on the long-chain conformational properties of the polystyrene molecules and their interaction with the latex particle interface. By this argument, we show that a model with surface excess of monomer near the particle surface is indeed more plausible than a homogeneous model. Figure 32 depicts a latex particle containing 25% polymer i.e., at equilibrium saturation, in which monomer and polymer are uniformly distributed. The preferred thermodynamic conformation of the styrene polymer molecule is the random coil. Typically a polymer chain will occupy an effective spherical volume some two or three hundred angstroms in diameter. In a uniformly distributed latex particle, only those molecules with their centers of mass near the center of the particle will be able to occupy random-coil conformations. Thus, a central region of the latex particle will be comprised of a loosely entangled network of polymer chains all occupying their preferred random-coil conformations — which is a normal condition of equilibrium at the molecular level for an amorphous polymer such as polystyrene. In a particle that is, say 2000Å in diameter, about 30% of the polymer segments will be located in a 100Å-thick shell, and it is to this shell (Figure 32a) that we now draw your attention. As we

Figure 32

Entropic considerations
75% monomer, 25% polymer

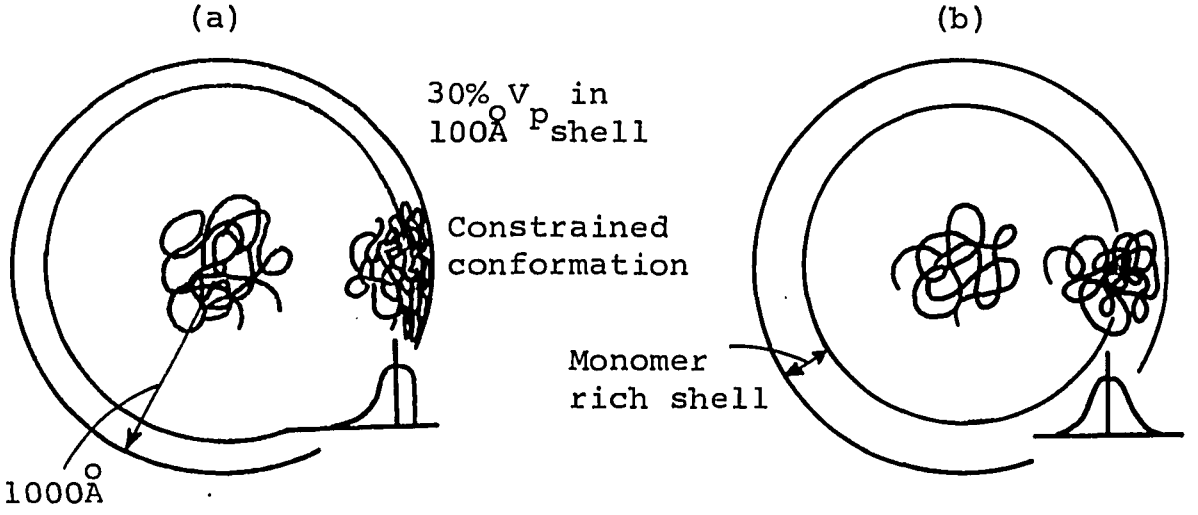

Homogeneous particle with low degree of conformational freedom and low entropy

Encapsulation model with a high degree of conformation freedom and high entropy

Heuristic model for the encapsulation phenomenon based on entropic considerations. In both sketches a molecule located in the central region is able to occupy its most favorable conformation —— that of an essentially random coil. In sketch (a) for a particle with a uniform segment density distribution, the molecules near the periphery will necessarily assume constrained conformations. In sketch (b) for an encapsulated particle, molecules near the periphery will tend to locate as far from the interface as is necessary to achieve a favored conformation.

have attempted to depict in the figure, a molecule whose center of mass is located within this hypothetical shell cannot occupy its preferred conformation. About one-half of its chain segments would be distributed "normally" on the inner side of the particle with a near-Gaussian distribution, but the other half would be "compressed" against the impenetrable particle-water interface with a "squared-off" distribution. The net result would be an unusually low conformational degree of freedom and a correspondingly low entropy for a polymer molecule near the particle periphery. As depicted in Figure 32b, a more entropically favored particle would consist of a central region with a dense network of entangled, coiled polymer chains plus some monomer, and a peripheral region with a dilute network of polymer chains which would occupy their most favored conformations.

The foregoing argument is also thermodynamically satisfying. Consider the Gibbs free energy, G, with $\Delta G = \Delta H - T\Delta S$. For polystyrene-styrene systems, ΔH is small and negative; for stable systems ΔG is negative and tends to minimize, whereas ΔS is positive and tends to maximize. Now ΔS depends on randomness and thus the number of available conformational states. The most random systems are the most stable; and for polymer systems these are the systems with the highest degrees of conformational freedom. The

polymer molecules in the distributed structure in Figure 32b have more conformational freedom associated with them than those in Figure 32a. Hence, from an entropic point of view, the former is more stable and the preferred state for a latex particle at equilibrium saturation. This assumes that the conformational freedom contributes more to the overall entropy than the entropy of mixing - which will decrease in a distributed (separated) system. We in fact show in Appendix III, using the calculations of D. J. Meier (8) that the free energy of restricted volume can be considerably greater than the free energy of mixing.

This analysis also suggests that the latex particle morphology is part of a larger class of problems: namely, polymer-chain conformations at interfaces, in both microscopic and macroscopic systems. Such considerations dominate the behavior of the microscopic latex particle systems because of the large surface to volume ratios associated with such systems. This notion is in accordance with our expectations, that the core-shell model should be evidenced over all ranges of particle sizes.

A. Restricted Volume Effects

We next present a theoretical argument to show that an encapsulated structure with a polymer segment density distribution is more likely than a uniformly distributed system. This argument is based primarily on the concept of a free energy of restricted volume as outlined by D. J. Meier (8). Also relevant in establishing a physical model is the work of van den Hul and Vanderhoff (10) and Ottewill (11). They showed that the SO_4^- endgroups — a result of persulfate initiation — tend to remain on the surface of the latex particle. The distribution of segments within the particle will be governed by the desire of the individual chains to occupy their most favored (random coil) conformations. Recall that in macroscopic solution polymer chains tend to pervade a volume which is in excess of 200Å in diameter. In the crowded and confined habit of the latex particle many of them will be prevented from doing so — namely, those near the particle-water interface. Figure 32 attempts to depict this situation. Molecules near the center of the particle will be able to occupy more favored states than those near the periphery.

With the heuristic argument in mind let us now consider the results of Meier's work. He calculated the free energy of restricted volume, $\Delta G_v(\delta)$ of a polymer molecule between two

plates separated by a distance, δ, compared to the free energy if the plates were infinitely separated. In this analysis the molecule is attached to one place at one chain end. For a flexible long chain molecule, such as polystyrene, random flight statistics are applicable. The required chain statistics are generated by the diffusion equation

$$\frac{\partial W(\bar{r})}{\partial N} = \frac{\ell^2}{6} \nabla^2 W(\bar{r}) \tag{5}$$

for $W(\bar{r})$ the probability of the end-to-end distance being $\bar{r}$, for N segments of length ℓ.

As the surface containing the attached chain is brought closer to the other surface, the volume available to the chain decreases; and, as a result, certain chain conformations will be excluded. At a separation distance δ, the fraction of allowable chain conformations will just be equal to the probability $P_N(\delta)$ that all elements of the attached chain are within a distance δ of the surface when the other surface is at infinity. This probability can be determined from the diffusion equation as follows. First obtain the conditional probability $W_N(x,r;x',0;\delta)dV$ of finding the free end of the chain of N segments in the volume element dV at x,r in cylindrical coordinates when the first end is at x=x' and r=0. The boundary conditions for this problem are

$$W_N(0,r;x'0;\delta) = W_N(\delta,r;x',0;\delta) = 0 \qquad (6)$$

These conditions also exclude from the ensemble those conformations for which any of the segments has reached the boundaries at x=0 or δ.

The solution to Equations (5) and (6) is normalized for $\delta = \infty$. Since we want the first chain end to be at x=0 we let $x' \to 0$. With the solution for $W_N(x,r;0,0;\delta)dV$, we find $P_N(\delta)$ as follows

$$P_N(\delta) = 2\pi \int_{r=0}^{\infty} \int_{x=0}^{\infty} W_N(x,r;0,0;\delta) r dr dx \qquad (7)$$

From the Boltzmann relation

$$\Delta G_V(\delta) = -T\Delta S_V(\delta) = -kT \ln (P_N(\delta)) \qquad (8)$$

The result obtained is as follows

$$\frac{\Delta G_V(\delta)}{kT} = -\ln \sum_{m=-\infty}^{m=+\infty} \left\{ \exp\left[\frac{-6m^2\delta^2}{N\ell^2}\right] - \exp\left[\frac{-3(2m-1)^2\delta^2}{2N\ell^2}\right] \right\} \qquad (9)$$

which is shown graphically in Figure 33. From this result it is seen that if a long chain molecule is confined in too small a space, i.e., $\delta \to o$, a large positive free energy would result rendering that situation thermodynamically unlikely.

Figure 33

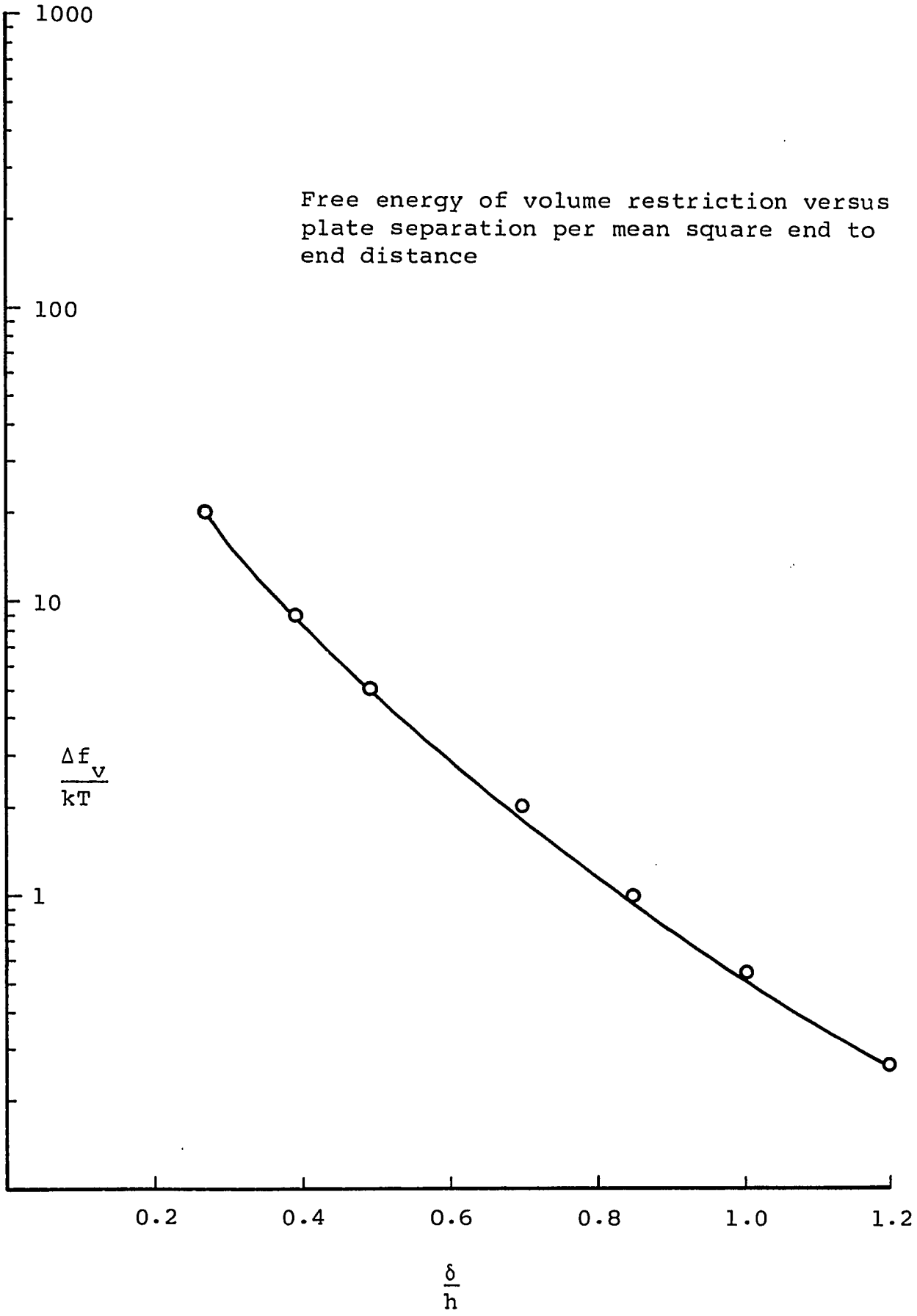

Free energy of volume restriction versus plate separation per mean square end to end distance

The analogy between the situation Meier depicts and the uniformly distributed latex particle of Figure 33 is clear. To avoid segmental compaction the center of mass of these long chain molecules must be a significant distance away from the surface so as to allow the polymer chains to enjoy more favored conformations and, consequently, have a lower free energy. Thus, a distributed structure with a low segment density in the vicinity of the interface is more likely than a uniformly distributed system.

B. Distributions Near an Interface

Since we are concerned with the polymer-segment distributions near the latex water interface, we now consider in a general way the segment distributions for a polymer chain located near an impenetrable flat interface, allowing for segment adsorption at the surface. For this adsorption problem of a flexible polymer at an interface with possible interaction energy, we refer to the work of DiMarzio and McCrackin (7). They determine the segment density distributions for long chain flexible molecules, which have one chain-end fixed to a surface, as a function of distance, molecular weight, and attractive energy of the surface. Monte Carlo methods were used in the execution of their

Figure 34

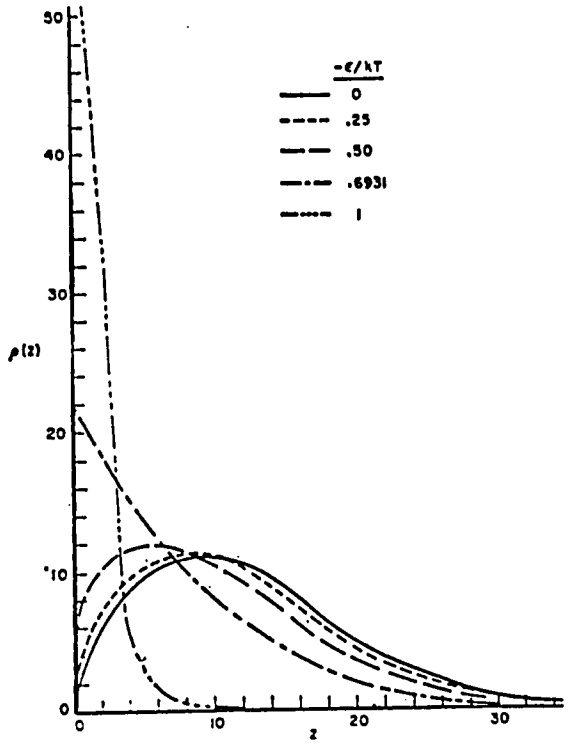

Distribution of density ρ(z) of polymer segments versus distance z from the surface for various values of adsorption energy for chains of 200 segments. For adsorption energies less than the critical value of kT $\ell n 2$, the curves have similar shapes and pass through a maximum. For adsorption energies greater than 0.693kT, most segments lie close to the surface (7).

calculations.* Figure 34 displays the polymer segment density as a function of distance from the surface for various values of attractive energy; Figure 35 shows the average number of segment contacts at the surface as a function of attractive energy with chain length as a parameter. The pertinent feature of their results is that for energy values of $-\epsilon/kT <$ ca. 0.6 the polymer segment density $\rho(z)$ approaches zero and the number of adsorption contacts approaches one.

The low values for adsorption contacts and segment density for values of $-\epsilon <$ ca. 0.6kT indicates that there is very little polymer near the surface even for systems where the interaction energy is of the same magnitude as the energy associated with van der Waal's type forces. The result for $\epsilon=0$ is particularly interesting. One can calculate the mean square end-to-end distance, $\bar{R}^2$, by means of the Ballot theorem (45). The number of paths (conformations) of a polymer of N segments is given by

$$P(N,z) = \left(\frac{2}{\pi N}\right)^{1/2} \left[2^{N+1}(z+1)/N\right] \exp(-z^2/2N) \qquad (10)$$

* A maximum of two hundred steps were used in their calculations, which corresponds to the evaluation of a polymer of approximately 20,000 molecular weight. This relatively low number of steps is adequate for our problem, since the conformational properties generated at this number have been found to differ very little from those conformational properties that could be calculated by theory at infinite molecular weight.

Figure 35

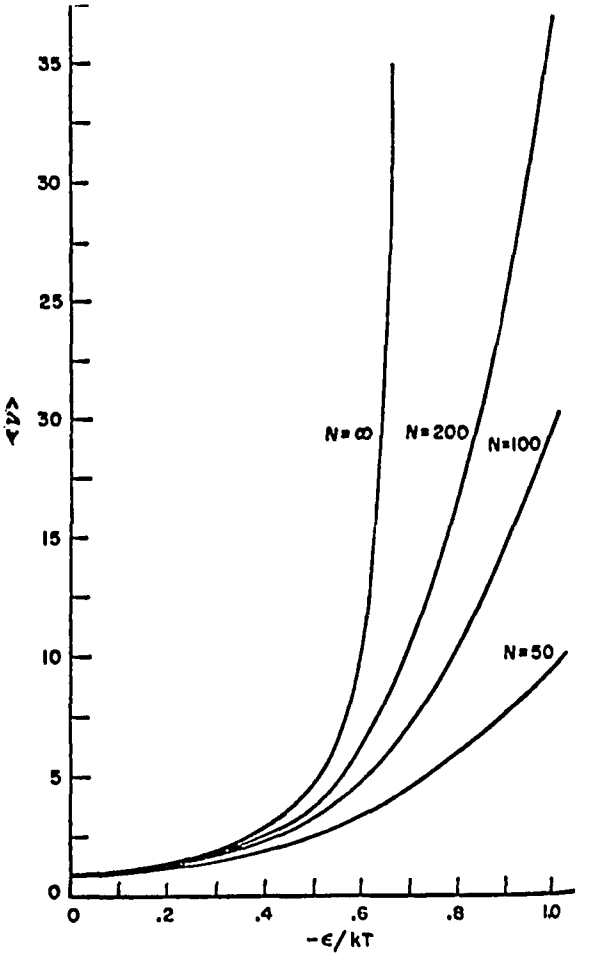

Average number ‹ν› of contacts with the surface versus the energy of adsorption in units of kT for chains of 50, 100 and 200 segments. The theoretical curve for infinite chain lengths (∞) is also shown (7).

$\bar{R}^2$ is then calculated as follows

$$\bar{R}^2 = \int_0^\infty z^2 P(N,z)\,dz \;/\; \int_0^\infty P(N,z)\,dz \;=\; 2N^* \qquad (11)$$

The resulting mean-square end-to-end distance is twice that of the same polymer in the absence of an interface. Thus, the wall, in effect forbids all conformations from crossing it, thereby giving preference to conformations on just one side of the wall. Since many conformations that would have crossed the wall are forbidden, there will be a low segment density near the wall and the maximum segment density will shift away from the wall.

The experimental evidence produced for the styrene-polystyrene latex system under study shows that there is low concentration of polymer in the peripheral region of the latex. (Recall from the kinetic studies that the reaction takes place in the peripheral region and is first order with respect to essentially pure monomer [M]. Furthermore from our oil soluble initiator work most of the polymerization was found to occur in the periphery; despite the fact that initiator is everywhere within the swollen latex particle). This behavior would be expected for systems with low values of interaction energy ($-\epsilon/kT < 0.6$). Based upon the organo-chemical structures in the system under investigation, we

---

*Unit segment length is considered here.

would expect the interaction to be minimal. We cannot conceive of the polystyrene segments participating in any kind of hydrogen bonding or chem-adsorption with the hydrophilic interface or its surfactants. In fact, polystyrene, like most hydrophobic polymers, would be expected to be repelled by water as evidenced by its large contact angle. We conclude that for our system the adsorption energy of polymer segments with the surface is probably low. We use this conclusion in the next section where a model is presented that predicts the polymer segment density distribution for a monomer swollen high molecular weight latex particle that has a nonpenetrating noninteracting boundary.

C. Polymer Segment Density Distribution in the Latex

We now consider the plausibility of several segment density distributions for a polystyrene latex particle saturated with monomer — ca. 75 wt-% monomer. As has already been indicated, a uniformly distributed system of monomer and polymer is excluded. The kinetic evidence first cited in proposing the encapsulation phenomena could be reconciled by a model consisting of a pure polymer core surrounded by a pure monomer shell (4). Such an extremely distributed structure can be rejected on two counts. Van den Hul and Vanderhoff and Ottewill have shown that for persulfate

initiated styrene emulsion polymerization nearly all of the polymer chain ends are located on the surface. If the bulk of the polymer is located in the core and the polymer chain ends tend to locate on the surface, then polymer chain segments must be present in the intervening monomer layer.

A pure polymer core can be excluded as well. Saturation seeding experiments of the sort described earlier with sufficient butadiene -- ca. 10% -- to introduce polymer-polymer incompatibility and the oil soluble initiator runs are the bases for this assertion. With reference to incompatibility effects, Figure 23b shows an ultra-thin cross-section obtained for such an experiment. The core-shell structure is clearly evident. One can also observe dark grains in the core which are attributable to the polymer-polymer incompatibility introduced during the second generation of polymer growth. That is, some of the 90/10 styrene/butadiene comonomer mix must have located in the core region during saturation and polymerized <u>in situ</u> to produce a copolymer incompatible with the polystyrene of the first generation core. As for the oil soluble run, the shell obtained after repolymerization is smaller than expected indicating that some polymerization occurred in the core which gives also evidence that monomer is associated with the core.

Evidence of monomer in the core and polymer in the shell have prompted use of the terminology "polymer-rich core", "monomer rich shell", and "high monomer concentration in the peripheral region" in describing the proposed core-shell morphology.

Based on this evidence a more likely distribution is suggested in Figure 32b. Here we depict a quasi two-phase system. The chain segment density $\rho(r)$ is high in the center and drops off sharply to form a well defined interface between the core and shell zones.

A fourth possible distribution follows from further theoretical work by Meier (9). The only assumptions required to establish our model for the latex particle are that end groups are fastened to the surface, that random flight statistics are applicable and that there is no significant adsorption energy between polymer segments and the surface. The required chain statistics are generated by the diffusion equation for $W(N, \bar{r}, \bar{r}', R)$, the probability of finding the free end of a chain of N segments at $\bar{r}$ with the fixed end at $\bar{r}'$. R is the particle radius. The appropriate boundary condition for chains confined to the interior is

$$W(N, R, \bar{r}', R) = 0 \qquad (12)$$

which also excludes from the ensemble those conformations in which any segment has reached the boundary at R. The segment density, ρ of a single chain of σ_A segments is obtained by summing W over N

$$\rho(\sigma_A;\bar{r},\bar{r}',R) = \sum_{N=1}^{\sigma_A} W(N;\bar{r},\bar{r}',R) \qquad (13)$$

The total segment density $\Omega(\sigma_A;\ \bar{r},\ R)$ is the sum of the number densities ρ contributed by each chain in the particle with the chain origin $\bar{r}'$ fixed at the surface.

This problem has been treated by Meier for spherical domain formation in block copolymers (9). It has been shown that the angular dependence of segment density becomes negligible for more than 24 chains whose origins are equidistant from each other on the surface of the sphere. This is because of overlap of adjacent molecules. He has also shown that the normalized segment density is

$$\Omega' = \left(\frac{4\pi R^3}{3\sigma_A N_A}\right)\Omega \qquad (14)$$

where N_A, the number of chains, is independent of chain length for $\sigma_A > 20$ and negligibly dependent on placement of the chain end for $r'/R > 0.9$.

Figure 36 curve (a) shows Ω' as a function of radius

Figure 36

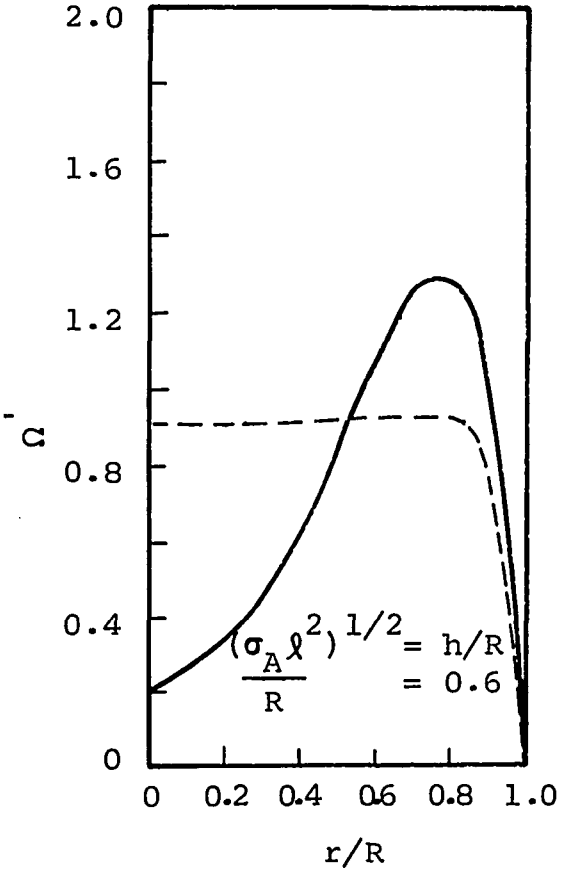

Relative density of segments for h/R = 0.6 (Reference 9).

r/R for $(\sigma_A \ell^2)^{1/2}/R$, the ratio of the root-mean-square end-to-end chain distance to the particle radius, equal to 0.6 (an intermediate value for the situation under consideration). The region of low density at the center of the particle is a region of very high energy and will not occur. It arises from the use of purely random-flight statistics and would be smoothed out by chain perturbations if the solution potential (free energy of mixing) were included in the calculation (a far more difficult problem). The effect of the wall is lost as one approaches the particle center, allowing unconstrained polymer segment-monomer mixing. This surface free mixing near the center will decrease free energy and smooth out central concentration gradients. The solution potential in effect pulls chain segments toward the center. The result is a nearly uniform density of segments over most of the particle which drops sharply to zero at the outer surface. Curve b of Figure 36 shows this distribution qualitatively. We now have a monomer-polymer distribution which shows a polymer-rich region near the center which sharply drops to a monomer-rich region near the interface. We believe that these theoretical considerations place the encapsulation phenomena on a firm theoretical foundation.

V. PRESENTATION OF AN ADVANCED MODEL FOR STYRENE EMULSION POLYMERIZATION

We have so far developed considerable insights into the factors controlling latex particle morphology in seeded polymerizations emanating from conditions of saturation equilibrium. The purpose of this section is to weave these insights into a coherent physical model for single charge growth from 0 to 100% conversion and to explain the kinetics of styrene emulsion polymerization in the most detailed manner now possible and to enhance the important Smith-Ewart, case 2 kinetic model for emulsion polymerization.

Let us briefly summarize the pertinent facts: (i) Grancio and Williams explained the extended Smith-Ewart case 2 kinetics observed from nucleation to 60% conversion in terms of a core-shell model for polystyrene latex growth, stating that the growing latex particle consists of a polymer-rich core and a monomer rich shell, with this shell serving as the major locus of polymerization. (ii) In this study a variety of styrene emulsion polymerizations were run starting from conditions of equilibrium saturation. These experiments conclusively confirmed the original model of Grancio and Williams and lead to the postulates that the core-shell mode of growth is governed by phase conditions

within the particle and that these conditions are similar to those at saturation equilibrium. (iii) The experimental work of van den Hul and Vanderhoff (10) and Ottewill (11) established that virtually all of the persulfate end groups are bound to the latex interface. This detail must be included in any plausible model for styrene emulsion polymerization. (iv) We then applied current statistical mechanics of the conformations of polymers attached to interfaces to the latex system under study and showed that an excess of monomer is predicted near the interface.

Based on the above four observations we wish to present an advanced model for the growth of a polystyrene latex particle from just after nucleation to completion. We use the kinetic data of Grancio, which is the most complete set of kinetic data generated to date for styrene emulsion polymerization.

The advanced model is introduced by following the growth of the polystyrene latex particle from just after nucleation to completion. A detailed growth profile for Grancio's 21%/hr. run is shown in Figure 37. (His 13%/hr. run follows an essentially identical pattern.) The radius R_o of the unswollen latex particles corresponds approximately to the core diameter and is known over the entire range of conversion. From radius R and the dynamic weight fraction of

Figure 37

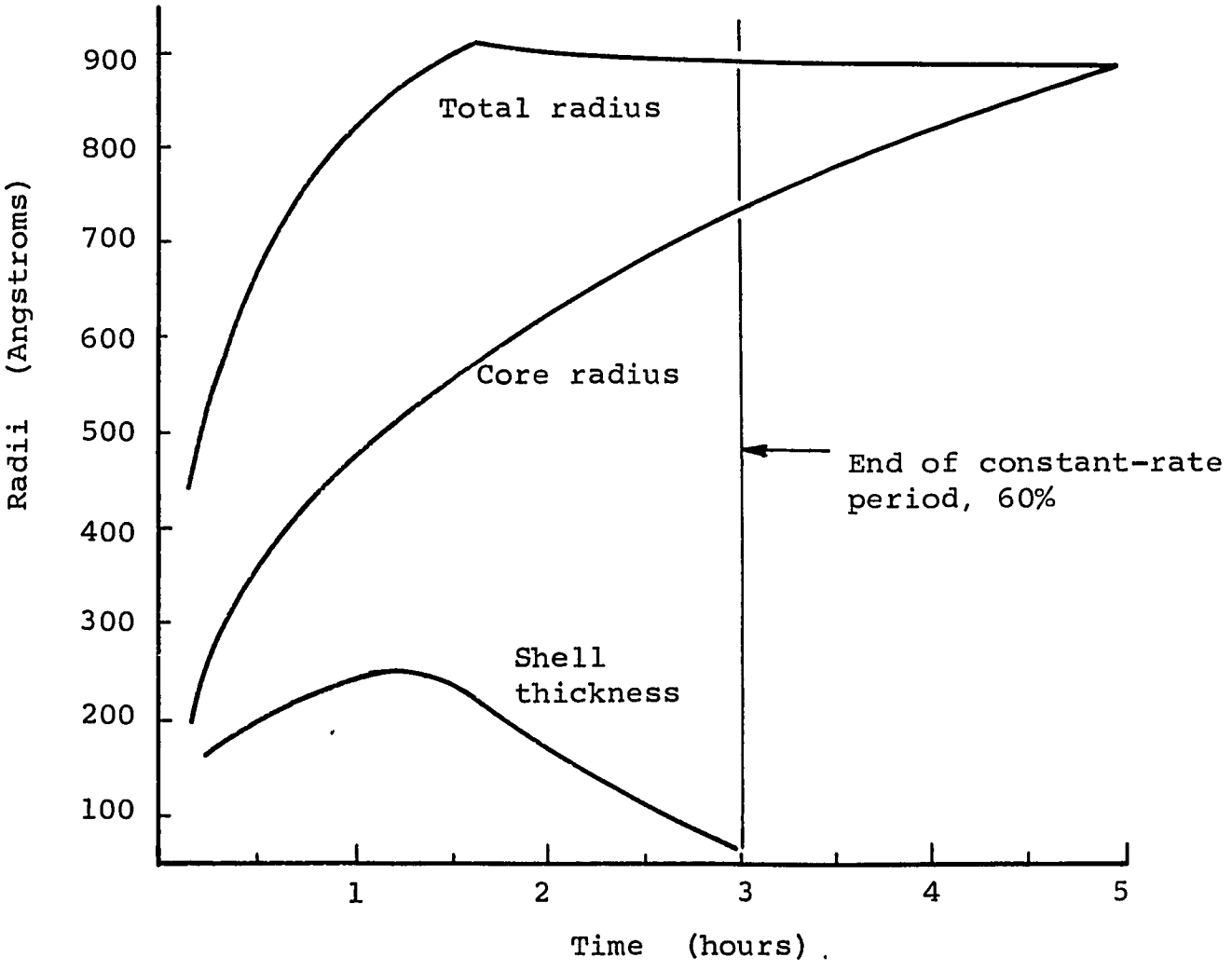

Growth profile of a latex particle at 21%/hour.

monomer, $[M]_w$, one calculates the outer particle radius R' of the monomer encapsulated latex with

$$R' = [R_o^3(\rho_p\mu/\rho_m + 1)]^{1/2} \quad (15)$$

where μ = the monomer-polymer ratio, $[M]_w/(1-[M]_w)$, ρ_p = polymer density and ρ_m = monomer density. The shell thickness, δ^*, is calculated by difference based on complete core-shell separation.

Observe in Figure 37 that the core grows continuously while the entire particle reaches a peak size at 30% conversion where the emulsified monomer disappears. The shell thickness increases at first and then shrinks after 30%. At 100% the core attains a radius slightly less than the peak radius because of density differences between monomer (0.905) and polymer (1.06).

First consider the period from nucleation to 60% conversion. Since only monodisperse formulations were used, nucleation occurs almost instantaneously near time zero. It is known from the dynamic runs where butadiene was spiked into the reactor just moments after nucleation that a growing polymer chain even in these early stanges of polymerization (ca. 500Å) grows to give a core-shell structure

* This is the calculated thickness of the pure monomer shell under the hypothetical condition of complete phase separation. It represents the maximum possible thickness of the shell.

when examined at completion.

In accord with spiking at 20% conversion, Grancio and Williams have shown constant rate behavior to 60% conversion, and concluded that Smith-Ewart case 2 kinetics prevails to this point. At this juncture we then have the picture of just one active chain growing in an outer zone of essentially pure monomer, with one end of this chain anchored to the particle water interface. Upon the entry of a second (oligomeric) radical into the particle, termination occurs very rapidly by combination. We present an explanation for this instantaneous termination in accord with the encapsulation phenomenon.

Prior to the finding of Grancio and Williams, constant rate behavior (constant R_{pp} in equation (2)) observed after the disappearance of monomer droplets was attributed to the fortuitous balance of increasing $\bar{n}$ and decreasing $[M]_w$. The notion that $\bar{n}$ increases beyond 1/2 as the reaction proceeds beyond small particle sizes and low conversions is founded on the presumed manifestation of volume and/or viscosity effects. The former is based on a probability argument in which the probability of a particle containing two free radicals increases with particle size, but this contention could only apply up to 30% conversion where the volumetric particle growth ceases. The viscosity effect is based on

the well-known Trommsdorf effect. With a core-shell structure, the reactor-volume consists of a relatively thin shell (e.g., for a particle 1600Å in diameter with $[M]_w$ = 0.75, the outer shell is at most 300Å thick), and its fluidity remains high to prevent the onset of a diffusion controlled termination mechanism. Consequently, if the growing particle has a core-shell structure instantaneous termination will occur in a very small and fluid shell reaction zone thereby allowing constant rate of growth to be maintained over an extended range of conversion.

Our theoretical considerations predict polymer segment deficiency near an inpenetrable interface and our seeded polymerization experiments emanating from conditions of equilibrium always show a core-shell structure. Thus, we suggest that core-shell behavior with peripheral growth should occur beyond 60% as well as before. The theoretical arguments presented predict <u>equilibrium</u> distributions of monomer and polymer segments within the swollen latex particle. The seeded polymerizations, starting from conditions of equilibrium saturation, upon electron microscope analysis of sliced sections at 100% conversion, always show the core-shell morphology. The core always corresponds to just the diameter of seed within experimental error (viz. Table III). These observations tell us that growth must occur just after equilibrium in the monomer rich outer zone in a manner depicted

schematically in Figure 38. In this figure we have attempted to pictorially describe the phase space within the particle. This phase space should not appreciably deviate from its condition at equilibrium as the reaction proceeds. The reaction "path" of a growing polymer chain will be in accordance with random flight statistics within the reaction zone. Since the polymer is moving randomly within the constraints of the system it should obtain a conformation similar to the one it would have at equilibrium and it should not appreciably disturb the overall condition of the phase space. That is, during growth the particle should exist in a state of quasi-equilibrium.

At conditions approaching complete conversion the phase space should change in character; but we next show that peripheral growth should still occur under this circumstance. Consider the core-shell mode of growth from a molecular kinetic point of view by comparing the time scales for polymer growth and diffusion. This argument should hold for all times. Consider an oligomeric free radical entering the distributed monomer-polymer particle as in Figure 38a. At 65°C it will take ca. 6.9 sec. on the average for the oligomer to become a high polymer of 10^6 molecular weight in essentially pure monomer. It is also known that polymer self diffusivity is dependent on its molecular weight to the

Figure 38

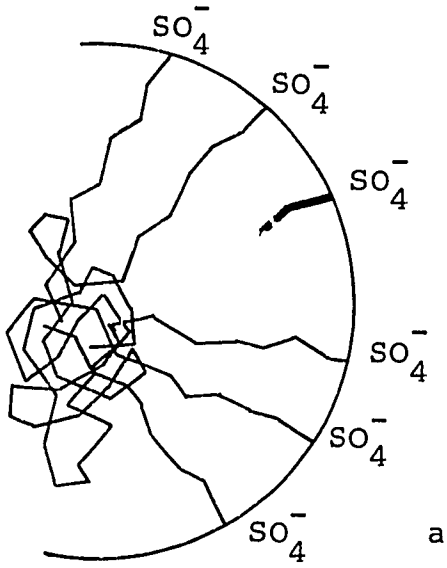

polymer dilute region

a. Oligomeric radical entering monomer-polymer particle

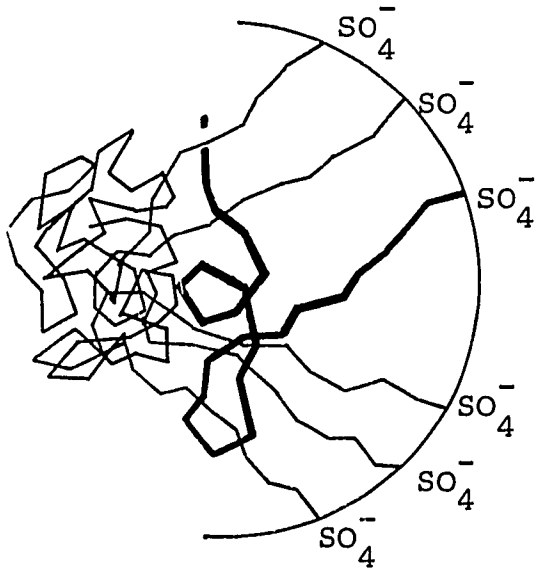

growing chain

b. Growth of radical in monomer-rich peripheral region

Model for core-shell growth in monomer swollen latex

-3.5 power (46)

$$D = KM^{-3.5} \tag{16}$$

If use is made of the fundamental definition of the diffusion coefficient

$$D = \frac{\bar{X}^2}{2t} \tag{17}$$

where $\bar{X}^2$ is the mean squared diffusion distance the center of mass of a molecule moves in a time t, one can determine the time it would take for the new polymer molecule to move 100Å into the existing polymer dense core. Using a polymer self diffusivity of 0.1×10^{-12} cm^2/sec (46,47) one obtains about 0.5×10^{33} seconds. Clearly then, within the course of reaction, it is impossible to obtain any significant amount of interpenetration of polymer and peripheral growth must occur during the entire reaction.

VI. DISCUSSION AND CONCLUSIONS

The focal point of this dissertation has been the core-shell model, introduced by Grancio and Williams to explain constant rate styrene emulsion polymerization (4,5). Their model was proposed on the basis of limited data obtained over a narrow range of experimental conditions. Hence, the first objective in this work was to verify the core-shell postulate and to establish the range of conditions over which it might apply. This objective was met in a series of seeded styrene emulsion polymerizations in which the second stage of growth was initiated only after the monomer II charge had reached equilibrium saturation with the seed polymer I. The location of polymers I and II in the final latex was ascertained by two methods of tagging: trace-butadiene and tritiated-styrene. In accord with the initial postulate, we found that polymers I and II were not uniformly mixed throughout the final particle but that polymer II overcoated polymer I in a core-shell fashion. This phenomenon prevailed despite the fact that sufficient time was allowed for swelling (48 hours) and that all the components were mutually compatible. We further found (using trace-butadiene tagging) that the core-shell morphology prevails over a wide range of conditions pertinent

to emulsion polymerization and latex technology: namely (i) molecular weight (from 0.02×10^6 to 10×10^6, viscosity average), (ii) particle diameter (from ca. 500Å to 6500Å), (iii) initiator type (water soluble and oil soluble), and (iv) butadiene level in polymer II (from 0.7 wt-% to 50 wt-% based on monomer II).

In order to explain these experimental facts, we have suggested that a structure similar to the core-shell structure exists even at equilibrium saturation. That is, polymer I locates in the central region of the swollen particle and monomer II tends to concentrate at the periphery where it polymerizes after reinitation. For convenience, we refer to the structure at saturation as the encapsulation model —— which infers monomer encapsulation of the swollen seed —— to distinguish it from the core-shell morphology observed at complete conversion. The validity of the core-shell model is firmly rooted in experimental fact, whereas the encapsulation phenomenon is a postulate still to be conclusively verified by direct experimental observation. It has considerable indirect experimental support, and a theoretical basis which we are about to summarize.

In developing an explanation for the encapsulation phenomenon, we first note that the swollen latex particle

constitutes a microscopic and not a macroscopic thermodynamic system, and that we cannot expect macroscopic laws and observations to apply without suitable modification. Another way of viewing the situation is that we are dealing with a colloidal system which has a very high interfacial area to volume ratio and that we should expect this property to strongly influence, if not control, the distribution of monomer and polymer within the particle. Finally, in terms of the requisite factual information, recall that the polymer chain ends are largely bound to the particle surface. In terms of theory we have applied a number of general developments pertaining to the conformational behavior of polymer molecules bound by their chain-ends to an impenatrable, noninteracting surface. Others have shown for such a boundary condition —— random-flight statistics prevailing —— that the polymer chains tend to distribute with their centers of mass well away from the surface (7,9). This situation leaves the surface region rich in solvent. We have argued that the analogy to the swollen latex particle is straight forward. This analogy suggests that the polymer segment density distribution for a saturated latex particle is high in the central region, low in the peripheral region, and virtually zero at the interface, leaving the particle

monomer-rich in the peripheral zone. Thus, the encapsulation phenomenon has considerable theoretical support.

The technological implications of the preceding findings were explored for those systems in which monomer II is compatible with polymer I, but polymer II is not. In order to produce incompatibility in our systems, the butadiene content in the monomer II saturation charge was raised from 0.7 wt-% to 50 wt-% for polymerizations beginning with polystyrene seed. The core-shell morphology prevailed, and fine structure was observed in the form of a high concentration of butadiene around the core and/or as core inclusions. Such fine structure has been observed for commercial ABS latexes, and it has its analog in bulk polymerized impact polymer systems. The effect of fine structure on polymer physical and mechanical properties has only been partially explored. We have argued that the observed core-shell morphology in these systems is controlled by the encapsulation phenomenon while the fine structure is probably controlled by the inherent incompatibility between polymers I and II (9).

The core-shell morphology was originally postulated on the basis of kinetic studies of constant-rate styrene emulsion polymerizations. It would seem, in turn that the observations we have made should have strong inferences as to the factors controlling the kinetics. First we have shown that the

encapsulation model explains and enhances the important Smith-Ewart case 2 kinetics. We have also suggested that the core-shell model prevails during the entire reaction cycle and not from just zero to 60% as initially postulated. That is, during growth, the latex particle exists in a state of quasi-equilibrium and the same factors that govern the morphology at true equilibrium also govern it during polymerization.

At this juncture, the two most pressing problems are (i) to verify the encapsulation phenomenon in situ and (ii) to extend its applicability to other monomer (solvent)-polymer pairs. Another pertinent problem is to advance our understanding of the core-shell model's technological implications.

Perhaps the most appropriate way to study the morphology of latexes in saturation with monomer (or solvent) would be in situ, i.e. with the saturated particle in aqueous suspension but without repolymerization. Light scattering and NMR offer two possible approaches. Light scattering looks particularly promising since the necessary theory (scattering from concentric spheres with different indices of refraction) is well developed (48). Two difficulties might arise with this approach: a solvent with a sufficiently different index of refraction from the seed polymer might be difficult to

find, and the boundary between the central and peripheral zones may be sufficiently diffuse to obfuscate the scattering pattern.

One might be able to derive information via NMR about morphology and molecular conformations within latexes by an *in situ* study of the relaxation processes of saturated latexes. Deuterated water and a non-protonated solvent would have to be used. Wide line and narrow line NMR should be applied to the problem.

If either or both light scattering and NMR are generally applicable with facility, they could be applied to investigating the prevalence of the encapsulation phenomenon in a variety of polymer-monomer (solvent) pairs as well as for a range of particle sizes, soap types, plus other variables.

In terms of its extension, we would expect core-shell growth to be a general occurence in emulsion polymerization, provided the system meets the following four requirements: (i) the monomer must be of low solubility in the aqueous phase, (ii) the polymer must be freely orienting (flexible), (iii) the initiating species should originate in the aqueous phase, with an entering oligomer anchoring at the interface by its hydrophilic chain end, and (iv) there should be low energy of interaction between polymer segments and the

interface. If the monomer or polymer has sufficient water solubility, one might expect the chain ends to penetrate into the aqueous phase, rendering the system more homogeneous, with new polymer growing well within existing polymer. Low polymer-interface interaction energy is necessary to obtain monomer surface excess. If initiation does not originate in the aqueous phase, but within the swollen latex particle, such as by use of a oleophilic initiator, then polymerization would occur throughout the swollen latex particle at rates dependent upon the distribution of monomer and initiator in the particle. Because of the higher concentration of monomer towards the periphery there would be more polymerization as one proceeds from the center to the interface —— as we have shown in the seeded polymerizations initiated by the oil soluble initiator benzoyl peroxide.

APPENDIX I: POLYMERIZATIONS

The emulsion polymerizations of styrene used in this work essentially followed the procedures of Woods et al. (19,31). Both single stage and multi-stage syntheses were used. The reactor consisted of a 300 ml bottle and polymerizations were conducted in a bottle polymerizer. Whenever tritiated styrene was used a glass 50 ml spherical reactor with a glass stirrer was used for the synthesis.

A. Materials

Commercial grade styrene inhibited to a level of 12T with hydroquinone, supplied by Hogen Solvents and Chemicals Corp., Garden City, N.Y., was generally used. The tritiated tracer styrene was supplied by New England Nuclear, Inc., Boston, Mass. It had a specific activity of 0.5 mCi/mg and was also inhibited to 12T with 4 tert butyl pyro-catechol. The styrene was sparged with nitrogen to remove dissolved oxygen which can inhibit the polymerization. The water was doubly distilled and also sparged with nitrogen to remove dissolved oxygen.

The surfactants were Siponate DS-10, sodium dodecylbenzenesulfonate of structural formula

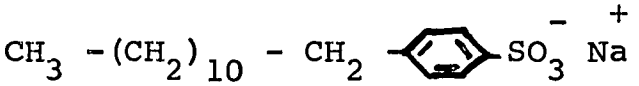

an anionic surfactant manufactured by Alcolac Chemical Corp., Baltimore, Md. and Triton X-100, a non-ionic octylphenoxy-ethanol with structural formula

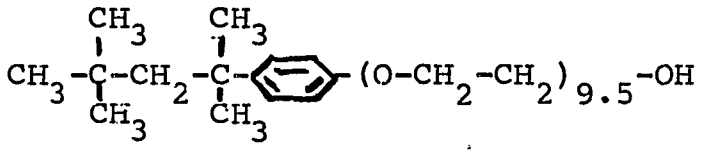

manufactured by Rohm and Haas, Philadelphia, Pa. Both surfactants were used as received.

The water soluble initiator was analytical grade potassium persulfate. The organic (oil soluble) initiator used in one run was analytical grade benzoyl peroxide.

The chemical stain receptor monomer, butadiene, was obtained by condensing butadiene gas obtained from a gas cylinder through copper coils immersed in a dry-ice-acetone bath. The liquid butadiene was then stored in a rubber gasket capped soda bottle in a freezer.

B. Reactors

1. Bottle Polymerizer

The bottle polymerizer consists of a covered stainless steel tank, 40 inches long by 25 inches wide by 30 inches deep, filled to a depth of 24 inches with water and insulated with asbestos board, plywood and canvas. The water is heated to a given temperature by means of two six-kilowatt Chromalox heaters. Temperature control is affected by means of an

on-off relay system connecting a temperature sensing element to the heaters.

The reactor bottles were held in cylindrical baskets which were bolted to wheels that rotated while submerged in the constant temperature water-bath. Specifically, the bottles were located on centers eight inches from the common axle of the wheels and tumbled end-over-end. The temperature was maintained at 65 ± 0.5°C. There were three wheels in the bath for a total accomodation of twelve bottles. The wheels were rotated at 25 rpm by a single speed motor.

The bottles were standard 12-ounce soda bottles. The bottles were sealed with an ordinary bottle cap and rubber gaskets. Before sealing, 1/16 inch holes were punched in the bottle cap so that materials could be added or removed during reaction by hypodermic syringe. Sealing was accomplished with laminated rubber gaskets consisting of circles of hard rubber and butyl-sealant rubber*. The circles were cut so that the hard rubber one fit just inside the cap and the butyl-sealant rubber just fit inside the bottle opening. These were then cemented together with Eastman 910 adhesive and placed inside the cap so that the smaller circle faced and covered the holes punched in the cap. After the gasket-cap arrangement had been pressed on the bottle, a few drops of toluene were placed over the holes in the cap to cause the

* Designated as "W-7" and "W-9" rubber, respectively, and obtained from B.F. Goodrich Co., Research Center, Brecksville, Ohio

butyl rubber to swell and effect a tight seal.

The formulations were charged to bottles cleaned in cleaning solution, washed with distilled water and dried. In general all ingredients were added gravimetrically. The distilled water and Triton X-100 were first added to the bottles on a Sartorius top loading balance capable of weighing to 0.01 gram. The Siponate DS-10 and sodium hydroxide were weighed on a Sartorius electronic analytical balance capable of weighing to 0.0001 gram. These materials were then transferred to the bottle. When the surfactants were completely dissolved in the water, the styrene was added. The potassium persulfate was weighed on the analytical balance and transferred to the bottle. The bottle was capped and butadiene was added, if called for, by hypodermic syringe and needle (20 gauge). The fully charged sealed bottle was placed in the bottle polymerizer which was preheated to its required temperature.

Care was taken to always fill the bottles with 300 ± 2 gram ingredients to insure that approximately the same level was used for every run so that dynamic equivalence would be maintained from run to run. In addition it was found that the 300 gram level gave the best conditions of agitation so as not to cause serious coagulation. Excess agitation, such as allowing a run to continue to turn in the bottle

polymerizer after 100% conversion (greater than 12 hours) lead to coagulation. This was not a serious problem since the latex would restabilize upon the addition of water.

2. Small Glass Reactor

A 50 ml glass reactor with ground glass top (24/40, SGA F4355) manufactured by Scientific Glass Apparatus, Inc., Bloomfield, New Jersey was utilized to produce all the tritiated materials for this work as listed in Table IV. The reactor was fitted with an airtight Chesapeake stirrer seal (SGA S7117) through which a specially made glass stirrer manufactured by Eck and Krebs, Inc., L.I.C., New York was inserted. The stirrer was rotated at 202 rpm by a G.K. Heller lab stirrer system. The reactor with about 25 ml total charge was immersed up to its neck in a stirred oil bath at 65 ± 0.1°C. A schematic diagram of the entire reactor system is shown in Figure 39.

The operation of the reactor follows. The required ingredients were placed in the reactor cleaned with cleaning solution, thoroughly washed with distilled water and dried. The order of addition was always : water, surfactants, sodium hydroxide, seed mixture (in a seed-overcoating run), styrene and initiator. The reactor mouth was then placed around the seal in which the stirrer shaft was inserted so as to have the stirrer blade bottom about 1.5 cm from the bottom

Figure 39

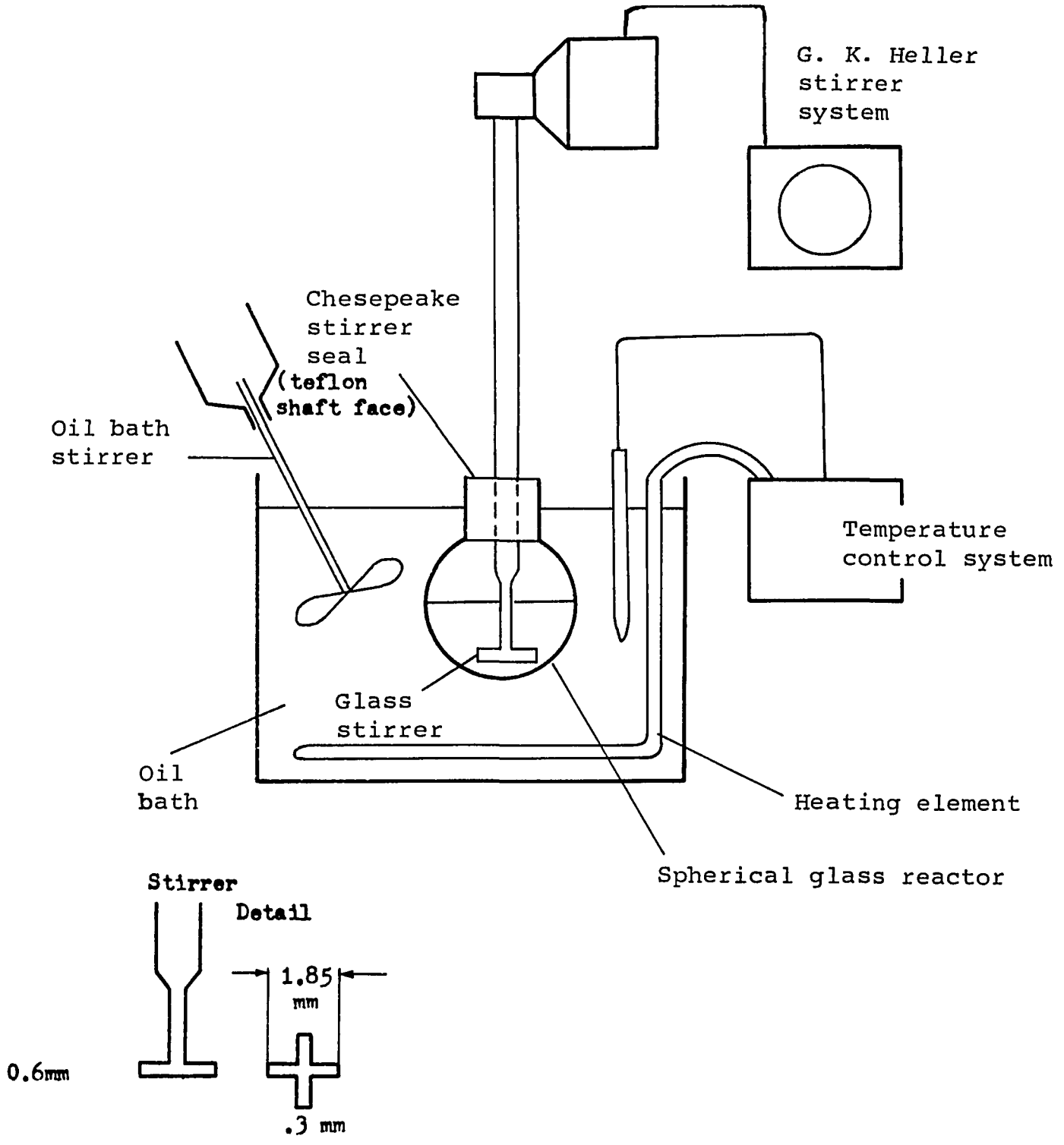

Schematic of small glass reactor apparatus.

of the reactor when stirrer shaft and seal and seal and reactor ground glass fitting were all sealed. The glass shaft, now coupled to the reactor was then coupled to the stirrer motor which automatically placed the reactor in the preheated oil bath. The reactor neck was clamped to a stand to prevent its rotation. The stirrer motor was then quickly brought up to proper speed as measured by a tachometer. The stirrer motor was run for at least a half hour before the reactor was connected to insure that the motor system was sufficiently warmed up at the start of the reaction.

C. Formulations

Two basic formulations are presented: one for the production of an ordinary seed latex and the other for the production of a two-stage overcoated latex from the seed.

1. Seed Formulation

The weight percentages are given in Table AI in order of addition to the reactor.

Table AI. A Standard Seed Formulation

Ingredient	Weight %
Water	53.40
Triton X-100	1.54
Siponate DS-10	.077
Sodium Hydroxide	.013
Potassium Persulfate	.076
Styrene*	44.88

*0.7% of the styrene contained butadiene.

2. Two Stage Overcoated Latex

Monomer was added to the seed latex to give a latex particle diameter increase of 50%. The monomer added based upon an added weight of seed latex charge, W_{ch}, is given by

$$M' = \theta_c W_{ch}\left(\left[\frac{D_f}{D_i}\right]^3 - 1\right) \tag{18}$$

where θ_c = weight fraction of latex in seed charge = 0.4488

D_f = diameter of final sized particle

D_i = diameter of initial sized particle

and $D_f/D_i = 1.5$

Surfactants were added to the seed latex mixture to give a 60% final surface coverage of surfactant. This was done to suppress second generation growth, since excess surfactant would tend to nucleate new particles. Added surfactant, based on added weight of seed latex charge W_{ch} is

$$Y = \theta_s W_{ch}\left(\frac{A_f}{A_i}\left[\frac{D_f}{D_i}\right]^2 - 1\right) \tag{19}$$

where θ_s = weight fraction of surfactant in seed

A_f = fraction area of final latex covered with surfactant

A_i = fraction area of seed covered with surfactant

and $A_f/A_i = 0.6$

Of the total amount of surfactants added, 0.925 was of the nonionic kind. The water content was 50%* of the final charge. The initiator content was set to 0.1% of the water in the final charge. No attempt was made to adjust for the content of any residual initiator left in the seed. With the final charge made up to be 300 grams, the water to be added, H_A, is given by

$$H_A = \Theta_W(300) - \Theta_H W_{ch} \tag{20}$$

where

Θ_W = the desired weight fraction of water

= 0.5 in this case

Θ_H = the weight fraction of water in the seed charge

= 0.534 in this case

The total weight of charge added, W_{ch}, is calculated by adding the weights of all ingredients to total 300 grams.

$$300 = W_{ch} + M' + Y + H_A + I \tag{21}$$

Substituting all quantities in terms of W_{ch} and solving gives the total amounts of ingredients to make up a 300 gram charge for a seed, overcoated run. These results are presented in

* In some runs, the water content was set to greater than 50% to aid stability.

Table AII in order of addition to the bottle reactor.

Table AII.

Two Stage Particle Formulation

Symbol	Ingredient	Weight (grams)
H_A	added water	97.97
Y	surfactants	
	(1) Triton X-100	0.5101
	(2) Siponate DS-10	0.0414
W_{ch}	seed charge	97.43
M'	styrene	103.86
I	initiator	
	potassium persulfate	0.15

Appendix II. TRACER CONCENTRATION CALCULATION

The low energy β particle emitter tritium is ideal as the tagging agent since it emits the weakest energy β particles and will therefore have the maximum sensitivity for autoradiography. We wanted to obtain a reasonable number of counts in the autoradiogram in a reasonable amount of time*. The prediction of the number of recorded counts by observing silver grains on a photographic emulsion layered on to the surface of the specimen is a highly empirical endeavor. In general, many β particles go unrecorded. To compensate for this, we choose a specific activity (SA) in our seed latexes that would give 10 exposures in 62.5 days. We then developed our layered photo-emulsions after 63 days. It should be pointed out that in this procedure, we were concerned with the relative amounts of recorded traces from specimen to specimen due to the decrease in efficiency that would be caused by the placement of an inert shell over an active seed core. Absolute recorded traces compared to the theoretical amount of β particles emitted were of little concern in this work.

The specific activity was calculated as follows. Specific activity has the units of $\frac{\text{curies}}{\text{gram}}$. One curie is equal to 3.7×10^{10} disintegrations per second; then the observed silver grain counts P will be equal to

*Less than 3 months is required to insure against latent image fading.

$$P = 1/2\ [3.7 \times 10^{10} \times 3600 \times (SA) \times W_p \times E \times t] \qquad (22)$$

Where t is time in hours and E is the autoradiographic efficiency i.e., the number of recorded silver grains per actual disintegrations. This value was chosen as 1/10 based on independent work in similar systems (6). The factor 1/2 enters since 1/2 of the β particles travel in a direction opposite to the photoemulsion. The weight of the active latex particle is given by

$$W_p = \frac{4}{3} R^3 \rho_p$$

Where $R = 1520\text{Å}$

and $\rho_p = 1.05\ gm/cm^3$

Equation 22 yields a value of 0.065 mCi/mg. We in fact used a stock solution of tritiated styrene at 0.050 mCi/mg which should yield results of little difference than those for the calculated specific activity.

APPENDIX III. CALCULATION OF THE THERMODYNAMIC EFFECTIVE MONOMER SHELL THICKNESS

The following calculations demonstrate the effect of restricted volume on the formation of a monomer rich shell within a swollen latex particle. The calculations should be viewed as approximate due to the required assumptions concerning the use of the free energy of restricted volume and due to inherent weaknesses in current polymer solution thermodynamics (50).

To be certain we have a consistent set of data, we base the calculations upon a system we have synthesized and characterized. The pertinent data is summarized in Table AIII.

Table AIII. Physical Data on Standard Polystyrene Latex

Particle size, R'_{oo}	980 Å
Molecular Weight, viscosity average, $\bar{M}_v$	2.585×10^6
Molecular Weight, number average*, $\bar{M}_w$	0.783×10^6
Equilibrium Saturation Content (wt %), [M]	0.73

*Based upon $\bar{M}_v = \bar{M}_w$ and $\frac{\bar{M}_w}{\bar{M}_v} = 3.3$ (5)

The calculation proceeds as follows, from a mass of monomer and polymer in bulk at a given concentration [M], remove enough material to form a sphere of radius R. The sphere is to consist of a core of monomer and polymer and a shell of pure monomer, hence there will be a free energy of mixing $\Delta G_M'/RT$ resulting from this segregation. Since the long chain molecules are attached at their chain ends to the particle interface (10,11) and they are confined near a surface, there will be a free energy of restricted volume $\Delta G_V/RT$. Other free energies such as that of surface formation $4\pi R^2\gamma$ and placement of chain ends on the surface (9) will be constant in this analysis, since we are only concerned with variations within the swollen latex particle. Essentially, we are concerned with the effect demixing has in reducing volume restriction of the polymer molecules within the spherical domain.

We then have $\Delta G_F/RT$ of our transformation

$$\Delta G_F/RT = \Delta G/RT - (\text{external surface free energies}) =$$

$$\Delta G_M'/RT + n(\Delta G_V/kT) \qquad (23)$$

The $\Delta G'_M/RT$ term can be approximated by the classical Flory-Huggins equation

$$\Delta G'_M/RT = N'_1 \ln v'_1 + N'_2 \ln v'_2 + \chi v'_1 v'_2 \quad (24)$$

where

N'_1 = number of moles of monomer in core

N'_2 = number of moles of polymer in core

v'_1 = volume fraction of monomer in core

v'_2 = volume fraction of polymer in core

These mole numbers and volume fractions will be expressed in terms of the hypothetical shell thickness, δ, of pure monomer. These will in turn allow us to relate $\Delta G_F/RT$ to δ. Partitioning a single component near an interface is a valid thermodynamic operation; one can think of a surface phase separate from the bulk in accord with the ideas of Guggenheim (51). An approach such as this, in a lumped fashion allows one to determine a single free variable which can account for the effect interface has upon the free energy of the system.

The radius R of the swollen latex particle can be found by direct use of the definition of weight fraction of monomer

$$[M] = \frac{(4/3)\pi(R^3-R_{oo}^3)\rho_M}{(4/3)\pi(R^3-R_{oo}^3)\rho_M + (4/3)\pi R_{oo}^3 \rho_P} \quad (25)$$

where R_{oo} is the radius of the unswelled latex seed. With R known one can then partition the swollen system into a polymer core swollen with monomer to thickness R_o and a pure monomer shell of thickness δ.

$$R_o = R - \delta \tag{26}$$

The system is pictured schematically as follows

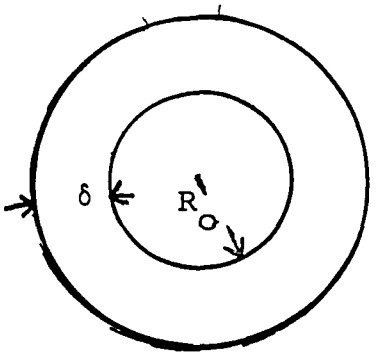

Relating the mole numbers to δ proceeds by material balance.

$$N_2' = \frac{(4/3)\pi R_{oo}^3 \rho_P}{M_2} \quad = \text{the moles of polymer, all in the core} \tag{27}$$

$$N_1'' = \frac{(4/3)\pi[R^3-(R-\delta)^3]\rho_M}{M_1} \quad = \text{the moles of monomer in the shell} \tag{28}$$

$$N_1 = \frac{1}{M_1}\frac{N_2' M_2 [M]}{1-[M]} \quad = \text{the overall moles of monomer in the system} \tag{29}$$

then

$$N_1' = N_1 - N_1'' \tag{30}$$

The volume fractions for Equation 24 are given as follows

$$v_1' = \frac{N_1'}{N_1' + \chi N_2'} \tag{31}$$

and $v_2' = 1 - v_1'$

where $\chi = M_2/M_o$ (32)

and M_o = molecular weight of a repeat unit

To calculate the second term of Equation 23, we assumed that n is equal to twice the total number of moles of polymer in the system, since all molecules are attached to the surface at both ends. The energy term ($\Delta G_v/kT$) is found directly from Figure 33 as a function of (δ/h), where h is the mean end-to-end distance of the polymer. We recognize that ($\Delta G_v/kT$) has been determined for planar geometry. We use it only because we do not yet have this function for spherical geometry. This value should be more pronounced in spherical systems, since curvature will restrict the polymer conformations in more than one dimension. The value of h is based on one-half the molecular weight of the polymer, since all

polymer chains are attached to the interface at both ends. For a polystyrene molecule of $\bar{M}_n = 0.220 \times 10^6$ in a good solvent, h_G, the mean radius of gyration, is 115Å (52). Since, $h^2 = 6h_G^2$, h for the system in question is

$$115 \cdot 6^{1/2} \sqrt{\frac{(1/2)(0.783 \times 10^6)}{(0.220 \times 10^6)}} = 382\text{Å}$$

$(\Delta G_F/RT)$ is tabulated versus δ in Table AVI and plotted in Figure 40 for values of [M] = 0.40 and 0.73. $(\Delta G_M/RT)$ used to calculate $(\Delta G_F/RT)$ is tabulated in Tables AIV and AV. It is seen that a minimum in free energy occurs at shell thickness values of 70Å and 90Å for the 0.40 and 0.73 values of [M], respectively. These "equilibrium" values of shell thickness place about 19.3% of the total monomer in the shell for the 0.40 case and about 35.6% for the 0.73 case. The foregoing calculations indicate that monomer-polymer separation in the swollen latex particle is the thermodynamically stable state rather than a homogeneous distribution of monomer and polymer corresponding to $\delta=0$.

δ	R_o	N_1''	N_1'	v_1'	v_2'	$-\Delta G_M'/RT$
(Å)	(Å)	moles$\cdot 10^{-16}$	moles$\cdot 10^{-16}$			$\cdot 10^{-16}$
10	1152	.01414	.2368	.3863	.6139	.1674
30	1132	.0407	.2107	.3590	.6410	.1604
50	1112	.0669	.1840	.3284	.6716	.1543
70	1092	.0920	.1589	.2970	.7030	.1471
90	1072	.1161	.1348	.2638	.7362	.1390
100	1062	.1278	.1231	.2465	.7535	.1343
120	1042	.1509	.1000	.2100	.7900	.1237
140	1022	.1730	.0779	.1715	.8285	.1108
150	1012	.1838	.0671	.1514	.8486	.1034
200	962	.2340	.0169	.0430	.9570	.0466

Table AIV. Change in free energy of mixing at swelling content [M] = 0.40 versus monomer shell of thickness δ.

δ	R_o	N_1''	N_1'	v_1'	v_2'	$-\Delta G_M'/RT$
(Å)	(Å)	moles$\cdot 10^{-16}$	moles$\cdot 10^{-16}$			$\cdot 10^{-16}$
10	1531	.0241	.9933	.725	.275	.2074
30	1511	.0720	.9454	.715	.285	.2066
50	1481	.1189	.8985	.705	.295	.2045
70	1471	.1640	.8534	.694	.306	.2046
90	1451	.2081	.8093	.682	.318	.2042
100	1441	.2300	.7874	.677	.323	.2029
120	1421	.2720	.7450	.665	.335	.2017
140	1401	.3132	.7042	.652	.345	.2016
150	1391	.3336	.6838	.645	.355	.2003
200	1341	.4299	.5875	.610	.390	.1962

Table AV. Change in free energy of mixing at swelling content [M] = 0.73 versus monomer shell of thickness δ.

δ (Å)	δ/h	$\Delta f_v/kT$	$\Delta G_v/RT$ $\cdot 10^{-16}$	[M] = 0.40		[M] = 0.73	
				$-\Delta G'_M/RT$ $\cdot 10^{-16}$	$\Delta G_F/RT$* $\cdot 10^{-16}$	$-\Delta G'_M/RT$ $\cdot 10^{-16}$	$\Delta G_F/RT$* $\cdot 10^{-16}$
10	.026	$> 10^5$	> 5.28	.1674	> 5.115	.2074	> 5.073
30	.079	10^5	5.28	.1604	5.120	.2066	5.073
50	.131	500	.0264	.1543	- .127	.2045	- .178
70	.183	70	.0037	.1471	- .143	.2046	- .201
90	.236	32	.0017	.1390	- .137	.2042	- .203
100	.262	22	.0012	.1343	- .133	.2029	- .202
120	.314	14.5	.0008	.1237	- .123	.2017	- .201
140	.366	10	.0005	.1108	- .110	.2016	- .201
150	.393	8.6	.0005	.1034	- .103	.2003	- .200
200	.524	4.2	.0002	.0466	- .0462	.1962	- .200

* $\Delta G_F/RT = \Delta G_v/RT + \Delta G'_M/RT$

Table AVI. System free energy $\Delta G_F/RT$ comparing free energy of restricted volume to that of mixing versus reduced shell thickness at [M] = 0.40 and 0.73.

Figure 40

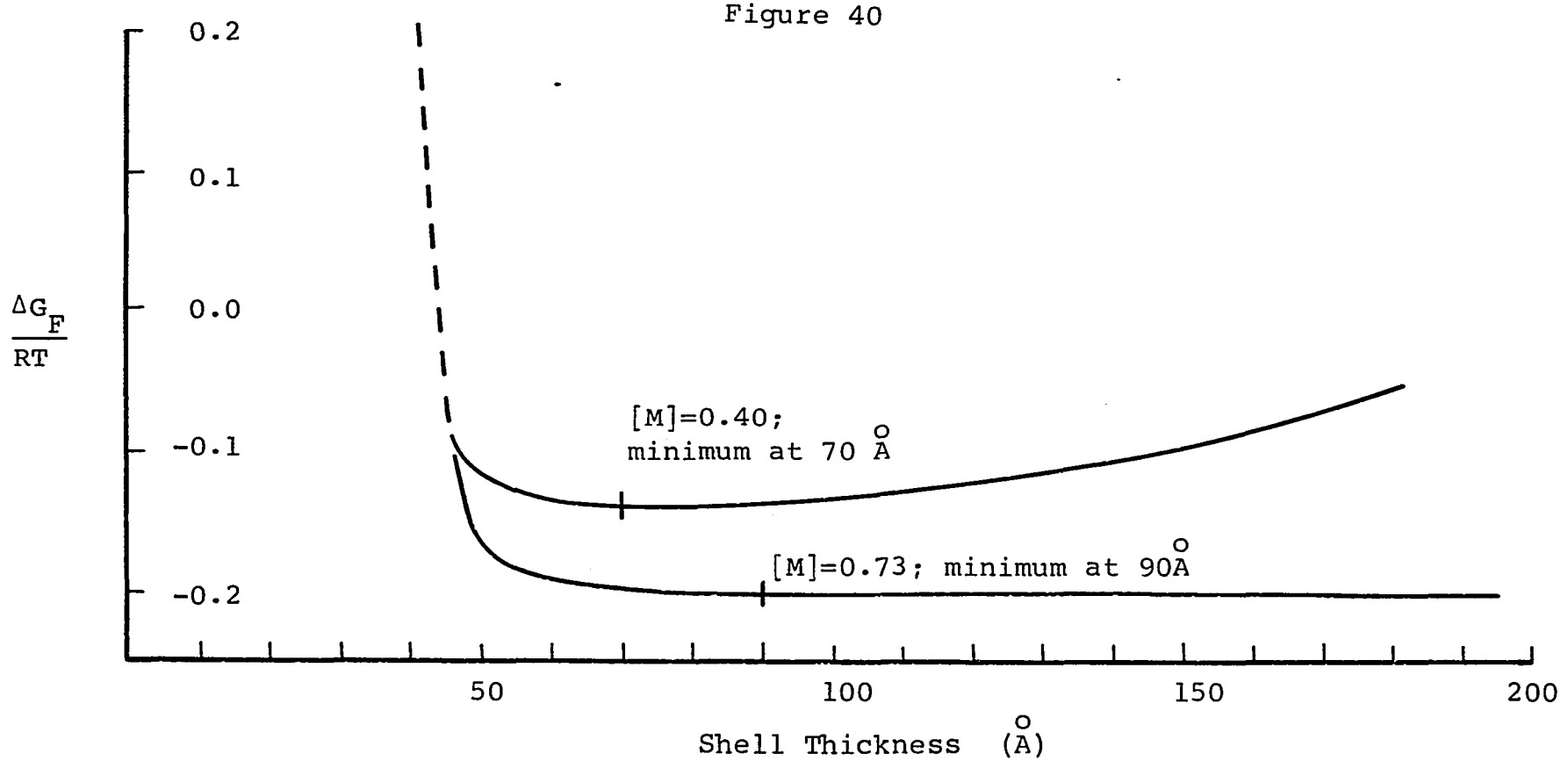

Free energy curves showing a minimum for $\delta \neq 0$ for two monomer concentrations. Curves are an approximation based on an extrapolation of data in Figure 33 to low values of δ.

BIBLIOGRAPHY

1. Smith, W.V., and Ewart, R.H., J. Chem. Phys., 16, 592 (1948).

2. Smith, W.V., J. Am. Chem. Soc., 70, 3695 (1948).

3. Harkins, W.D., J. Am. Chem. Soc., 69, 1428 (1947).

4. Grancio, M.R., and Williams, D.J., J. Polymer Sci., A-1, 8, 2733 (1970).

5. Grancio, M.R., "A Kinetic Study of Monomer-Polymer Ratio and Molecular Weight Development in Ideal Styrene Emulsion Polymerization", Ph.D. Thesis, The City University of New York (1969).

6. Rodgers, A.W., "Techniques of Autoradiography", Elsevier, New York (1969).

7. DiMarzio, E.A., and McCrakin, F.L., J. Chemical Physics, 43, #2 (1965).

8. Meier, D.J., J. Chemical Physics, 71, 1861 (1967).

9. Meier, D.J., J. Polymer Sci., Part C, 26, 81 (1969).

10. van den Hull, J.J., and Vanderhoff, J.W., Br. Polymer J., 2, 121 (1970).

11. Ottewill, R., University of Bristol, personal communication.

12. Bovey, F.A., Kolthoff, I.M., Medalia, A.I., and Meehan, E.J., "Emulsion Polymerization", Interscience, New York (1955).

13. Litt, M., Patsya, R., and Stannett, V., J. Polymer Sci., A-1, 8, 3607 (1970).

14. Williams, D.J., and Bobalek, E.G., J. Polymer Sci., A-1, 4, 3065 (1966).

15. Williams, D.J., and Grancio, M.R., J. Polymer Sci., C, 27, 139 (1969).

16. Vanderhoff, J.W., et al., J. Polymer Sci., 20, 225 (1956).

17. Laranger, A.H., Serafini, T.T., Von Fischer, W., and Bobalek, E.G., Official Digest, 31, #44, 482 (1959).

18. Serafini, T.T., and Bobalek, E.G., ibid., 32, #10, 1259 (1960).

19. Woods, M.E., et al., J. Paint Tech., 40, #527, 71 (1968).

20. Smith, W.V., J. Am. Chem. Soc., 70, 3695 (1948).

21. Smith, W.V., J. Am. Chem. Soc., 71, 4077 (1949).

22. Gardon, J.L., J. Polymer Sci., A-1, 6, 2859 (1968).

23. Vanderhoff, J.W., et al., J. Polymer Sci., 50, 265 (1961).

24. Gardon, J.L., J. Polymer Sci., A-1, 6, 623, 643, 665, 687 (1968).

25. Stockmayer, W.H., J. Polymer Sci., 24, 319 (1957).

26. Gerrens, H., Z. Eletrochem., 60, #4, 400 (1956).

27. Gerrens, H., Agnew. Chem., 71, #19, 608 (1959).

28. Napper, D.H., J. Polymer Sci., A-1, 9, 2089 (1971).

29. Williams, D.J., J. Polymer Sci., A-1, accepted for publication, November, 1972.

30. Herzfeld, S.H., et al., J. Polymer Sci., 5, 207 (1950).

31. Woods, M.E., et al., J. Paint Tech., 42, #541, 71, (1970).

32. Pease, D.C., "Histological Techniques for Electron Microscopy", Academic Press, New York (1964).

33. _____, "Instructions for Embedding Tissue in Epon 812 Based on Luft's Procedure", Ladd Research Industries, Inc., Burlington, Vermont.

34. Sjøstrand, F.S., "Electron Microscopy of Cells and Tissues", Academic Press, New York (1967).

35. Prescott, D.M., ed., "Methods in Cell Physiology", Volume II, Chapter 9, "General Area of Autoradiography at the Electron Microscope Level", by M.M. Salpeter, Academic Press, New York (1966).

36. Meek, G.A., and Moses, M.J., J. Roy. Microscop. Soc., 81, 187 (1963).

37. Prescott, D.M., ed., "Methods in Cell Physiology", Vol II, Chapter 10, "High Resolution Autoradiography", by A.R. Stevens, Academic Press, New York (1966).

38. Kato, K., Japan Plastics-Quarterly, 2, 6 (1968).

39. Bradford, E.B., and Vanderhoff, J.W., J.Polymer Sci., Part C, #3, 41 (1963).

40. Maron, S.H., J. Appl. Polymer Sci., 5, 282 (1961).

41. Vanzo, E., Marchessault, R.H., and Stannett, V., J. Colloid Sci., 20, 62 (1965).

42. Morton, M., et al., J. Colloid Sci., 9, 300 (1954).

43. Sperling, L.H., et al., Chapter in "Polymer Networks: Structural and Mechanical Properties", Chompoff, A.J., and Newman, S., Eds, Plenum Press (1971).

44. Adamson, A.W., "Physical Chemistry of Surfaces, 2nd ed., Chapter II, John Wiley and Sons, New York (1967).

45. Feller, W., "Introduction to Probability Theory and its Applications", 2nd ed, Chapter III, John Wiley and Sons, New York (1957).

46. Bueche, F., "Physical Properties of Polymers", Chapter 3, Interscience, New York (1962).

47. Odian, G., Keusch, P., et al., "A Study of the Synthesis of Hemodialysis Membranes", Final Report for National Institute of Health, Contract PH 43-67-1442, (1968).

48. Kerker, M, "The Scattering of Light", Academic Press, New York (1969).

49. Krieger, I.M., Case Western Reserve University, personal communication.

50. Flory, P.J., "Principles of Polymer Chemistry", Cornell University Press, Ithaca, New York (1953).

51. Guggenheim, E.A., Trans. Faraday Soc. 36, 397 (1940).

52. Tanford, C., "Physical Chemistry of Macromolecules", John Wiley and Sons, Inc., New York (1961).

VITA

Preston Keusch was educated in the New York City school system. He received his Bachelor's and Master's degrees in Chemical Engineering from the City College of New York. In 1964, after receiving his Bachelor's degree he worked as a process engineer for Wallace and Tiernan Inc. In 1965 he joined the staff of RAI Research Corp. where for the next six years he participated on a diverse variety of polymers related research and development projects. At RAI, he was Principal Investigator on studies evaluating the basic properties of crosslinked polyethylene, the synthesis and characterization of semipermeable membranes for hemodialysis and the development of continuous methods to irradiate thin polymeric films. In 1970 he came to the City University to work as a Research Assistant under Professor David J. Williams on an NSF grant. While at the college he has lectured for the Chemical Engineering Department in the area of polymer science. He plans to continue his career in the area of polymer science.